INSTITUTE FOR FUSION STUDIES

DE-FG05-80ET-53088-708 IFSR #708

Pulse Dynamics in an Unstable Medium

N.J. BALMFORTH
Institute for Fusion Studies
The University of Texas at Austin
Austin, Texas 78712 USA
G.R. IERELY
Scripps Institute of Oceanography
Univ. of California, San Diego, CA 92093
and R. WORTHING
Department of Mathematics
Massachusetts Institute of Technology
Cambridge, MA 02139

May 1995

THE UNIVERSITY OF TEXAS

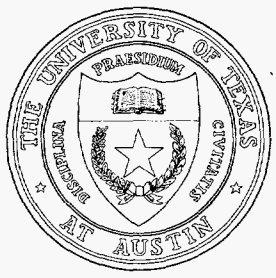

AUSTIN

DISCLAIMER

Pulse dynamics in an unstable medium[a)]

N. J. Balmforth,[b)] G. R. Ierley,[c)] and R. Worthing[d)]

Abstract

A study is presented of a one-dimensional, nonlinear partial differential equation that describes evolution of dispersive, long-wave instability. The solutions, under certain specific conditions, take the form of trains of well-separated pulses. The dynamics of such patterns of pulses is investigated using singular perturbation theory and with numerical simulation. These tools permit the formulation of a theory of pulse interaction, and enable the mapping out of the range of behavior in parameter space. There are regimes in which steady trains form; such states can be studied with the asymptotic, pulse-interaction theory. In other regimes, pulse trains are unstable to global, wave-like modes or *its radiation*. This can precipitate more violent phenomena involving pulse creation, or generate periodic states which may follow Shil'nikov's route to temporal chaos. The asymptotic theory is generalized to take some account of radiative dynamics. In the limit of small dispersion, steady trains largely cease to exist; the system follows various pathways to temporal complexity and typical bifurcation sequences are sketched out. The investigation guides us to a critical appraisal of the asymptotic theory and uncovers the wealth of different types of behavior present in the system.

Key words. Partial differential equations, chaos, nonlinear dynamics, singular perturbation theory, solitary waves

AMS(MOS) subject classifications. 34C35, 34C37, 35B25, 35A35.

[a)]This work was supported by the U.S. Air Force under contract number F49620-92-J-0061, and the U.S.D.O.E. under grant DE-FG05-80ET53088.

[b)]Institute for Fusion Studies, University of Texas, Austin, TX 78712

[c)]Scripps Institute of Oceanography, University of California, San Diego, CA 92093-0225

[d)]Department of Mathematics, Massachusetts Institute of Technology, Cambridge, MA 02139

I. INTRODUCTION

The dynamics of coherent structures plays an important role in the physics of a wide range of different systems. From moving interfaces in condensed matter physics to propagating solitary waves in fluids, the interaction of localized objects constitutes a fundamental issue. A theory of the dynamics of coherent structures is therefore of far-reaching and general utility, but here our goal is much more modest and precise.

Our aims in this paper are three-fold. Firstly, we consider the interaction of coherent structures in one of the simplest mathematical settings: pulse dynamics in one dimension. The particular physical system we study is one describing long-wave instability in a dispersive, nonlinear medium. In order to study the dynamics of the pulses, we use both numerical techniques and a formulation based on singular perturbation theory. An assessment of the utility and accuracy of this asymptotic method comprises the second aim of our study. Thirdly, the partial differential equation (PDE) we study undergoes various kinds of transitions to temporal complexity. In order to give a coherent study of this equation, we catalogue these various bifurcation pathways.

We begin with a PDE that arises in the fluid dynamics of thin liquid films[4]:

$$\partial_t u + u\partial_x u + \partial_x^2 u + \mu\partial_x^3 u + \partial_x^4 u = 0. \tag{1}$$

In this circumstance, $u(x,t)$ is the thickness of the film. Perhaps more importantly, equation (1) describes phase evolution in a translating frame for the complex Ginzburg-Landau equation, at least to within a small nonlinear term.[26] Hence the impact of our results extends to many spatially extended systems undergoing a Hopf bifurcation. In that context, $u(x,t)$ is the gradient of the phase of the order parameter. Previous studies have uncovered solitary wave solutions to the PDE (1);[28,13] these pulses constitute the central objects of our analysis.

The asymptotic method we employ to study dynamics assumes that the solutions to (1) are trains of widely separated, weakly interacting pulses. In an earlier work (hereafter paper I[3]) we gave a detailed discussion of this method in the context of constructing the steadily propagating solutions to (1). These steady pulse trains are the solutions to a third-order, ordinary differential equation (ODE). The asymptotic theory reduces the problem to an

algebraic relation between any one pulse separation within the train and its immediate successor. This can be viewed as a map of the interval into itself; a map intimately connected with a theorem of Shil'nikov.[35,36,38] In certain regions of parameter space the map guarantees chaotically spaced pulse trains, or spatial complexity. This spacing map is the main achievement of the asymptotic analysis of the equilibria. Here we follow the asymptotic recipe once again, but we do not restrict the motion of the pulses to be steady. Instead, the supposition that the train consists of weakly interacting pulses leads us to extract a set of coupled ODEs describing the evolution of the pulse positions; the equations of motion of the pulses.[12]

This asymptotic approach to pulse dynamics originates from studies on nonlinear field theories, reaction-diffusion systems and excitable media.[30,18,29] The distinction between the pulse dynamics of our system (1), and that of these earlier cases lies in the nature of the mechanism that creates the coherent structures. In nonlinear field theories, reaction-diffusion systems and excitable media, solitary pulses are typically generated by finite amplitude perturbations that exceed some threshold. In the long-wave equation (1), the homogeneous state, $u = 0$, or *vacuum state*, is intrinsically unstable. It is the amplifying instability that steepens into the pulse train for (1). This feature leads to some crucial differences in the dynamics associated with (1). In particular, it leads us to confront what we may call *radiative instability*; the instability of a solitary pulse through global, wave-like modes related to the unstable continuum of the vacuum state.

The main thrust of this paper is therefore to explore *radiative pulse dynamics*. In Sec. II, we give the standard, asymptotic formulation of pulse dynamics. Appendix A contains some important remarks concerning the ramifications of Galilean invariance on this theory. We compare the predictions of asymptotic theory with numerical calculations in Sec. III, which considers linear theory about simple equilibria. These comparisons highlight the importance of radiative instability, which motivates the extension of the asymptotic analysis presented in Appendix B. They also reveal regimes in parameter space in which we may be confident in the accuracy of the usual asymptotic theory. That observation, and the general importance of radiative instability, then motivate the more extensive numerical experiments of Secs. IV and V. Finally, in Sec. VI, we explore the limit of small dispersion, a regime of parameter space which contains various transitions to temporal complexity. Section VII concludes the study with some remarks about the implications of our results and some related issues. Some

preliminary calculations and discussion have appeared previously.[2,40]

II. SINGULAR PERTURBATION THEORY

A. Steadily propagating solutions

An important class of solutions to our PDE (1) are those that propagate steadily, $u(x,t) = U(x-ct)$, with some wave speed, c. These solutions satisfy the ordinary differential equation (ODE),

$$\left(\partial_\xi{}^3 + \mu\partial_\xi{}^2 + \partial_\xi - c\right) U + \frac{1}{2}U^2 = 0, \tag{2}$$

where $\xi = x - ct$ is a travelling-wave coordinate. In (2) and we have assumed that a constant of integration can be set to zero by suitably offsetting U and modifying c (this constant is fixed by selecting the Galilean frame in which we solve the PDE). Various solutions to this equation have been given elsewhere.[1,17,7,3] Of special interest are the solitary wave solutions, $H(\xi) = u(x,t)$, that represent localized pulses. If we regard (2) as describing the state of a dynamical system, the pulses correspond to homoclinic orbits in the phase space of this system that connect the origin, $U(\xi) = 0$ to itself as $\xi \to \pm\infty$.[2] The development towards a solitary pulse of a sequence of spatially periodic solutions with increasing period is shown in Fig. 1 (the limiting pulse shape is clearly apparent).

In paper I, we used singular perturbation theory to construct travelling-wave solutions in the form of pulse trains. These solutions consist of widely separated, weakly overlapping pulses. They have the approximate form,

$$u(x,t) = \sum_{k=1}^{K} H(x - ct - \xi_k) + \varepsilon\mathcal{R}(x,t), \tag{3}$$

for a train of K pulses centered at the positions ξ_k. The degree of error is measured as $\varepsilon = \exp(-\gamma\overline{\Delta})$ for $\overline{\Delta}$ a typical pulse separation, and γ signifies the characteristic exponent of the rate of the decline of the pulse amplitude to the front and back (assumed to be essentially the same). In order for the order ε correction, $\mathcal{R}$, to remain bounded, singular perturbation theory enforces a condition on the positions of all of the pulses. This solvability condition can be written as,

$$c_1 = F(-\Delta_{k+1}) + F(\Delta_k), \tag{4}$$

where c_1 is a constant speed correction,

$$\Delta_k = \xi_k - \xi_{k-1} \tag{5}$$

is the separation of the pulses, and the function

$$F(\Delta) = \frac{1}{\varepsilon I_0} \int_{-\infty}^{\infty} N(t)H(t)H(t+\Delta)dt, \tag{6}$$

with

$$I_n = \int_{-\infty}^{\infty} N(t)\frac{d^n H(t)}{dt^n}dt, \tag{7}$$

and $N(\xi)$ defined as the solution to

$$\left[\partial_\xi{}^3 - \mu\partial_\xi{}^2 + \partial_\xi + c - H(\xi)\right] N(\xi) = 0. \tag{8}$$

For large spacings, the function $F(\pm\Delta)$ has a dependence on Δ like the behavior of the tails of $H(\xi)$.

Equation (4) is the map of the pulse spacings; given Δ_k, we compute Δ_{k+1}, thence a pulse train.

B. Time-dependent pulse trains

For dynamics, we envision an array of widely separated pulses that mutually interact. Again, these pulses are assumed to overlap in their low-amplitude tails. The force exerted on a particular pulse by its immediate neighbors is therefore small, and leads to slow adjustments in the pulse positions. These ideas form the ingredients for weak-interaction analysis.

In equilibrium theory, the positions ξ_k are constants that become determined as a secularity condition on $\mathcal{R}$. In our theory of dynamics, we let the positions vary weakly in time to accommodate the slow adjustments mediated by interaction. This amounts to setting $\xi_k = \xi_k(\varepsilon t) = \xi_k(\tau)$, where $\tau = \varepsilon t$ is a slow adjustment timescale.

If we make a Galilean transformation into a frame moving with the speed of an individual pulse, the train is almost steady, and the only temporal dependence occurs through pulse adjustments and therefore τ. This transforms (1) into the PDE,

$$\varepsilon\partial_\tau u + \partial_\xi\left[\left(\partial_\xi{}^3 + \mu\partial_\xi{}^2 + \partial_\xi - c\right)u + \frac{1}{2}u^2\right] = 0. \tag{9}$$

Written in this form, the method outlined in paper I can be straightforwardly generalized to accommodate the evolution of the pattern. The singular perturbation theory then enforces a solvability condition,

$$\dot{\xi}_k = F(-\Delta_{k+1}) + F(\Delta_k), \tag{10}$$

which is an equation of motion for the position of the k^{th} pulse.[12]

III. PERIODIC EQUILIBRIA AND STABILITY

Periodic domains provide a convenient and informative setting in which we can solve the PDE (1). In such cases the pulse trains are comprised of periodic sections of length L, each of which contain N pulses.

In general, it is not possible to find analytically the exact, nonlinear periodic solutions to the PDE (1) and examine their stability. Instead, we use numerical techniques. Given a periodic solution $U(x-ct)$, stability can be determined by solving the equation,

$$\lambda v = \partial_\xi \left[\left(\partial_\xi{}^3 + \mu \partial_\xi{}^2 + \partial_\xi - c + U \right) v \right], \tag{11}$$

for infinitesimal perturbations of the form, $v(\xi) \exp \lambda t$. In the frame moving at speed c, the periodic solution is stationary, and (11) is a conventional eigenvalue problem (rather than a Floquet calculation). We solve (11) by introducing a Tchebyshev expansion in ξ, and truncating at some suitably large order (using the tau method to treat boundary conditions). This yields as many eigenvalues as there are rows in the truncated matrix, and gives a faithful representation of the low-order eigenmodes.

In asymptotic theory, we must supplement the equations of motion for the pulse positions (10) with the periodicity requirements,

$$\sum_{n=1}^{N} \Delta_n = L, \qquad x_1 + L = x_{N+1}, \qquad \Delta_{N+1} = \Delta_1. \tag{12}$$

Equilibria follow from the spacing map (4) and the above relations. The stability of such configurations is dictated by the linear eigenvalue problem,

$$\lambda d_k = -F'(\Delta_{k-1}) d_{k-1} + [F'(\Delta_k) + F'(-\Delta_k)] d_k - F'(-\Delta_{k+1}) d_{k+1}, \tag{13}$$

where λ is an eigenvalue and d_k is an infinitesimal perturbation in spacing, with the constraints,

$$\sum_{n=1}^{N} d_n = 0, \qquad d_1 = d_{N+1}. \tag{14}$$

This is an $N \times N$ tridiagonal matrix problem subject to the constraint (14). The solution consists of a zero eigenvalue and a set of nontrivial eigenvalues. The zero eigenvalue corresponds translation of the whole pattern in ξ, and also emerges as a solution to the full problem (11). The other eigenvalues correspond to relative displacements of the pulses within each periodic array.

A. Single-pulse states

Periodic solutions containing a single pulse compose the simplest kinds of pulse trains that we can consider. As solutions of the PDE (1), these single-pulse states are born in a supercritical Hopf bifurcation from the equilibrium or vacuum state, $U = 0$. This bifurcation occurs as the domain size L is increased through 2π, and signifies the destabilization of the wave, $\sin\xi$, with $c = \mu$. Beyond the bifurcation, the mode saturates at finite amplitude, and, on increasing L further, steepens into a pulse. As $L \to \infty$ the pulse develops into a solitary wave (see Fig. 1).

In Fig. 2, we display some properties of the stability of the single-pulse states. In panel (a), the stability is illustrated for the particular state $L = 40$ and $\mu = 0.5$. Displayed are the lowest eigenvalues in the complex plane; modes occur as a real solutions, or complex conjugate pairs. The behavior of the real parts of the lowest-order eigenvalues as L varies is plotted in the second panel, and a selection of eigenfunctions for $L = 40$ is drawn in the final panel.

For the single-pulse states, there are two real modes, one of which has a zero eigenvalue. That mode corresponds to a simple shift in the position of the pulses and arises from translational invariance. By differentiating the equilibrium equation (2), we observe that this mode must have the eigenfunction, $U'(\xi)$. Provided the domain is sufficiently large, the structure of the single-pulse state is almost that of a solitary wave, and $U'(\xi) \simeq H'(\xi)$.

The other real mode is relaxational in character; it arises at the birth of the pulse as the neutral mode transforming the equilibrium into the infinitesimal wave (Fig. 2(b)). We denote

its eigenfunction by $V(\xi)$. As L becomes large, the eigenfunction (somewhat surprisingly) takes on an appearance very much like $H'(\xi)$. The eigenfunctions of the real modes are localized to the vicinity of the pulse; they are examples of modes that are intrinsic to the shape of the pulse itself.

In addition to the real modes, the single-pulse states also have an infinite set of complex eigenmodes. The eigenfunctions of these modes are not localized, and, rather than being attenuated away from the core of the pulse, possess substantial amplitude there. As shown in Fig. 2(a), the eigenvalues approximately lie along the curve,

$$\nu = k^2(1 - k^2), \qquad \omega = k(c - Q + \mu k^2), \tag{15}$$

where k parameterizes the curve, and

$$Q = \frac{1}{L}\int_{-L/2}^{L/2} U(x)dx. \tag{16}$$

This curve emerges from a variational estimate of the eigenvalues with a trial solution, $\exp ik\xi$, assuming $k \gg 1$. In addition, for $k = 2\pi n/L$, $Q = 0$ and $n = 2, 3, 4, ...$, it is the dispersion relation for infinitesimal perturbations to the state $U = 0$. This observation suggests that the complex solutions are related to the normal modes of the vacuum state; that connection can be established more completely by tracing the eigenvalues as functions of L back to the critical domain size. In these senses, then, the complex eigenmodes are intrinsic to the vacuum rather than the pulse. In view of their oscillatory structure and finite frequency we call them radiation modes, following similar terminology in nonlinear field theory.[5,14]

According to asymptotic analysis, single-pulse states follow from the relation $F(L) + F(-L) = c_1$, which determines the speed correction for each L, and there is only a single, trivial stability eigenvalue. Thus asymptotic theory predicts that the single-pulse states are always stable. This highlights one of the main failures of the asymptotic theory; the omission of the radiation modes. It arises because the singular perturbation theory is founded on the idea of weakly interacting localized structures, whereas the radiation modes are global. An embarrassing consequence is that, in the limit of large spacing in which one would expect the asymptotic theory to be most accurate, large numbers of radiation modes bifurcate to instability (Fig. 2(b)), and the dynamics becomes dominated by them.

The failure of the asymptotic theory, whilst unappealing, is not completely surprising;[37,7] solitary wave solutions contain extensive regions over which the amplitude is very small. These regions are susceptible to the same instability that creates the pulses themselves.

B. Double-pulse states

The stability properties of some two-pulse states are illustrated in Fig. 3. These states are characterized by equal spacing, $\Delta_1 = \Delta_2 = L/2$ (there exists an infinite sequence of asymmetrical states with unequal spacing.[13]) Like the single-pulse states, the symmetrical double-pulse states bifurcate out of the vacuum when L increases through a critical value, in this case, 4π. In Fig. 3, we display the low-order portion of the spectrum for the state with $\mu = 0.4$ and $L = 40$, the behavior of the real parts of the eigenvalues with domain size, and a selection of eigenfunctions. The spectrum has much in common with the single-pulse state; it contains a small number of real modes, and an infinite set of radiation modes that bifurcate to instability for sufficiently large L.

Of the real eigenvalues, we can again identify the purely neutral mode. However, rather than a single mode of relaxational character, there are now three more real eigenvalues. The eigenfunctions of all the real modes are displayed in Fig. 3(d). It is clear from that picture that the real eigenfunctions are spatially localized to the pulse positions, indicating that they are all intrinsic to the pulses. This leads us to explain the presence of the modes as follows. Just as the two-pulse state can be approximately constructed by superposing two single-pulse solutions, we can construct its eigenfunctions by superposing the localized modes of the single-pulse state (*cf.* Ref. 5). The analogues of the translation and relaxation mode are, therefore, $H'(\xi-\xi_1)+H'(\xi-\xi_2)$ and $V_+ = V(\xi-\xi_1)+V(\xi+\xi_2)$ respectively. However, in linear theory it is not sufficient to create all solutions by an constructive superposition, since the localized modes may have arbitrary amplitude. The destructive superposition, $V_- = V(\xi-\xi_1) - V(\xi+\xi_2)$, and the individual translation, $S = H'(\xi-\xi_2)$, are also, therefore, permitted as linearly independent solutions. These four eigenfunctions comprise the real modes pictured in Fig. 3(d).

The mode $S(\xi)$ acts to translate the second mode and not the first. In other words, it pushes two neighboring pulses together, and the pairs on either side apart. These relative

displacements are the motions that are described by asymptotic theory. As is evident from Fig. 3(c), there is agreement between this eigenvalue, and the stability eigenvalue, λ, derived from asymptotic analysis, provided the domain is sufficiently wide. In the asymptotic limit, such compressional motions of the array of pulses are overdamped (Appendix A). Their resemblance to over-damped oscillations in a one-dimensional lattice of springs leads us to call the associated eigensolution, a "lattice mode." The eigenvalue associated with $S(\xi)$ is therefore the linear damping of the spring; the nonlinear behavior of this spring follows from asymptotic theory and equation (10).

Throughout most of the range of spacings pictured in Fig. 3, the relaxational modes are much more strongly damped than the lattice mode. However, it is clear from Fig. 3(b), that when Δ becomes too short, the eigenvalues of the lattice mode and V_- can become comparable. At that point, the modes actually collide and form a complex conjugate pair. This signifies a point at which perturbations of the shape of the pulses decay with critical damping. For smaller values of L, the system of pulses is underdamped and the effects of inertia become felt. The complex mode formed from the fusion of the two real solutions we denote by $M(\xi)$; for want of a better term, we call it an "inertial-mode."

The formation of the inertial mode amounts to a greater degree of freedom in the dynamics of the pulse interactions; it signifies the breakdown of the asymptotic theory at short spacing. Unlike the large-spacing limit, this regime is where one expects the theory to cease being valid, and is, therefore, rather less unsatisfactory. However, over a fairly wide range in the parameter space, (μ, L), the inertial mode actually becomes unstable. This lead to overstable pulse dynamics which we explore numerically in a later section.

IV. ACCESSIBLE DYNAMICS

The calculations of equilibria and their stability suggest that the asymptotic theory of pulse dynamics works within a fairly narrow range of spacing values. In Fig. 4, we give some idea of this range of validity, by plotting a "regime diagram" for the symmetrical, double-pulse states. In this figure, we sketch various bifurcation points on the $(L-\mu)$ plane. To the right, we encounter the Hopf bifurcation that signifies the inception of radiative instability. To the left, we plot the curve along which the lattice mode and $V_-(\xi)$ merge into a complex

eigensolution. The locus at which this mode bifurcates to overstability is also sketched.

If we lower the degree of dispersion in the system by reducing μ, the linear stability properties become more complicated, as the regime diagram suggests. In fact, below about $\mu = 0.1$, our classification scheme becomes a little ambiguous since we cannot always distinguish the inertial mode and radiative solutions. Moreover, even further towards the dispersionless limit, the modes we can trace to radiative solutions at larger μ, begin to split into real pairs, and the equilibria themselves no longer resemble distinct pulses. In addition, the asymptotic theory also fails for all spacing because pulses become asymmetrical.[3] At that point, then, it is no longer useful to use the terminology. In Sec. VI we continue to use the notation in the limit $\mu = 0$, but only when following bifurcation sequences from larger dispersion where there is no ambiguity.

A. Simple adjustments

According to the above arguments, it is only in the region of Fig. 4 marked "accessible," and for μ well away from zero, that we can hope that the asymptotic theory provides a reasonable description of the pulse dynamics. Here we have solved the PDE numerically[24] for a selection of values for μ and L. Typically, from a set of arbitrary initial conditions, the system evolves to a steady pulse train. More often that not, the relaxation proceeds too quickly in its initial stages to be captured by any weak interaction analysis (examples of this kind of evolution are given in Subsec. VI.A). The limit in which the asymptotic theory can be conveniently realized are the instances in which the system begins from a weakly disturbed, unstable equilibrium. That is, evolution from an equilibrium for which there is a mildly unstable lattice mode. The unstable train then relaxes slowly to a stable train. We call this kind of evolution a simple adjustment to distinguish it from the fast relaxations that, for example, violently create pulse trains out of very different initial states.

Figure 5 shows an adjustment from a slightly perturbed unstable state at $\mu = 0.7$ and $L = 28$. The unstable equilibrium is an asymmetrical double-pulse solution. The states to which the system evolves depends on the initial condition, but provided the initial perturbation is not excessively large, the outcome is one of two equilibria neighboring the unstable state in solution space. Four experiments are shown in Fig. 5; two approach the symmetrical state as

time proceeds, whereas the others decay into another train with more asymmetrical spacings. In the figure, we show the evolution projected onto the $\Delta - \dot{\Delta}$ plane. Although the PDE, when viewed as a dynamical system, has as many dimensions as there are modes used in the truncated spectral expansions, the evolution from all four initial conditions rapidly settles down to follow a well-defined curve which is accurately predicted by the one-dimensional ODE of asymptotic theory.

The experiments shown in Fig. 5 are a fairly favorable example for comparing numerical results with asymptotic calculations; the spacings are well within the "accessible" regime, and, for this value of μ, the pulse amplitude decays quite symmetrically. We show results in less favorable regimes in Figs. 6 and 7. Figure 6 shows an experiment at $\mu = 0.4$ and $L = 28$. In this calculation, the stable, asymmetrical two-pulse state possesses an eigenvalue of inertial-mode character. Consequently, the trajectory spirals into the fixed point in the $\Delta - \dot{\Delta}$ plane. Adjustment to the stable, symmetrical state is better predicted by the asymptotics, although the comparison is worsened by the asymmetry in the decay of the pulses amplitude at this value of μ.

The experiment shown in Fig. 7 lies close to the border of radiative instability. The initial disturbance excites the nearly neutral radiation mode, and it begins to "ring" persistently. As the state evolves towards a neighboring asymmetrical state, this mode passes parametrically through a Hopf bifurcation, and thereafter begins to grow exponentially. Throughout the evolution, the trajectory of the numerical solution follows a helical path. On average, it roughly shadows the asymptotic calculation, when projected onto the $\Delta - \dot{\Delta}$ plane, but the drift of the pulses is substantially accelerated by the radiation through its root-mean-square effect.

V. RADIATIVE DYNAMICS

Stability theory and experiments like that shown in Fig. 7 suggest that radiation modes play a primary role in the dynamics of pulse trains with relatively large spacings. An investigation of pulse train dynamics cannot therefore be complete without a study of the ramifications of radiative instability.

Very close to the border of instability, there is a single radiation mode that is nearly

neutral. Here, we can extend the asymptotic theory by including that mode as a further small perturbation. The details of the calculation are presented in Appendix B. Briefly, the eigenfunction, φ, and frequency, ω, of the marginal mode emerge as the solution to,

$$(\partial_\xi{}^4 + \mu\partial_\xi{}^3 + \partial_\xi{}^2 - c\partial_\xi)\varphi + \sum_{k=1}^{K} \partial_\xi(H_k\varphi) = i\omega\varphi, \tag{17}$$

where $H_k = H(\xi - \xi_k)$, and c is the solitary wave speed, and we have expanded the parameter, μ, about its marginal value, $\mu \sim \mu_0 + \varepsilon\mu_1$. We then modify the ansatz for the approximate pulse train,

$$u(\xi,t) \sim \sum_{k=1}^{K} H_k + \varepsilon^{1/2}[A(\tau)\varphi(\xi)e^{i\omega t} + \text{c.c.}] + \varepsilon\mathcal{R}(t,\xi,\tau) + \varepsilon^{3/2}\mathcal{S}(t,\xi,\tau), \tag{18}$$

where $A(\tau)$ is the amplitude of the radiation mode, and $\mathcal{R}$ and $\mathcal{S}$ are successive corrections in the asymptotic expansion. By scaling the amplitude of the nearly neutral mode by $\varepsilon^{1/2}$, we introduce the root-mean-square effect of the wave at the same order as the terms modelling long-range pulse interactions. This conjunction is encapsulated in the solvability condition,

$$\dot{\xi}_k = \tilde{\mu}_1 + F(\Delta_k) + F(-\Delta_{k+1}) + \alpha_k|A|^2, \tag{19}$$

with $\tilde{\mu}_1 = \mu_1 I_2/I_0$ and

$$\alpha_k = \frac{1}{I_0}\int_{-\infty}^{\infty} |\varphi(\xi)|^2 N(\xi - \xi_k)d\xi. \tag{20}$$

The amplitude of the radiation mode is found to evolve according to the relation,

$$\partial_\tau A = \varpi A + \rho|A|^2 A, \tag{21}$$

where ϖ and ρ are integrals given in Appendix B.

Superficially, equation (21) appears to be a standard type of Landau equation. Implicitly, however, φ depends on the set of pulse positions, $\{\xi_k\}$, thence τ. The coefficients, α_k, ϖ and ρ in equations (20) and (21), therefore give those ODEs a rather complicated non-autonomous character. In practical terms this means that the amplitude equations are somewhat time-consuming to solve. Because, in addition, the expansion is not likely to remain valid very far away the point of bifurcation, we have not explored the solutions to (20) and (21) in any detail. Nonetheless, the amplitude equations provide some insight into the phenomenon of radiative instability.

Equations (20) and (21) predict the emergence of a solution with finite-amplitude radiation;

$$c_1 = \tilde{\mu}_1 F(\Delta_k) + F(-\Delta_{k+1}) - \alpha_k |A|^2, \qquad |A|^2 = -\mathrm{Re}\ \varpi / \mathrm{Re}\ \rho. \tag{22}$$

This branch is either subcritical or supercritical depending on the sign of the real part of ρ. Just beyond the point of bifurcation, subcritical branches are unstable, and radiative instability precipitates a violent event. By contrast, supercritical branches are stable, and pulse trains with superposed radiation are realizable.

The coefficient ρ is plotted in Fig. 8 for single-pulse states on the verge of radiative instability. At larger values of μ, the coefficient has positive real part; there the radiative modes compose subcritical instabilities. At smaller values of μ, radiation saturates at finite amplitude. The switch from supercritical to subcritical bifurcation as μ increases also holds for double-pulse states, and we suspect it to be true for pulse trains in general.

The solution (22) remains valid only at relatively small amplitude. In order to continue the solution branches further, towards strongly nonlinear *radiative states*, we need to fall back to numerical techniques. Various solutions constructed using truncated Fourier expansions in both time and space are illustrated in Fig. 9. In panel (a), solution branches are portrayed according to the mean amplitude of the radiation mode, $\mathcal{A}$, defined by

$$\mathcal{A} = \left[\frac{1}{L\Pi} \int_0^L \int_0^\Pi (u - \langle u \rangle)^2 dt dx \right]^{1/2}, \tag{23}$$

where $\langle F(x,t) \rangle$ means average of the quantity at point x over one period, Π. The dashed lines at the base of the branches indicate the asymptotic solutions, (22), although in order to draw the branches against L, we expand about the critical domain size which leads to a slightly different form for ϖ than given in Appendix B (there we have expanded in μ to more clearly illustrate the asymptotic expansion). In Fig. 9(b), the finite-amplitude solution branches are plotted according to period.

The branches proceed from their bifurcation points to larger amplitude and longer period; various space-time surface plots of the solutions at three points along the branch for $\mu = 0.4$ are shown in 9(c), 9(d) and 9(e). The form of the collision between the radiation and the pulse is surprisingly similar to pictures of interactions in experiments with binary fluids.[16]

The branches are not continued further than the uppermost points shown in Figs. 9(a)

or 9(b) because the computations become laborious and expensive. The increasing period, various numerical experiments and the final space-time plot of Fig. 9(e) all suggest that the fate of the solution branches is a homoclinic bifurcation to an asymmetrical two-pulse state. The termination of the radiative solution branch is therefore an example of a nontrivial homoclinic orbit in a PDE.

To smaller values of μ, the structure of the branches become more complicated. In particular, the topology of the branches alters near $\mu = 0.3$, and the path to homoclinicity becomes less obvious, if it exists at all.

A. Subcritical instability and pulse creation

When the unstable radiation mode is subcritical, its amplitude grows destructively such that instability disrupts the original pulse train. In Fig. 10, we show the result of instability of the single-pulse state at $\mu = 0.8$. After a slow period of exponential growth, the instability suddenly amplifies rapidly, violently disturbs the pulse and eventually destroys it. The principal wavecrests of the radiation mode then emerge as pulses in their own right. Any remaining small-amplitude disturbances subsequently either damp out or collide with the pulses, leaving a steadily propagating, two-pulse state. (In Fig. 10, and all following figures portraying space-time evolution, we present the solutions in suitably moving frames to bring out their details.)

In Fig. 10, the weakly unstable radiation mode grows fairly slowly, but it triggers a relatively fast transition. Yet more violent transitions are shown in Fig. 11. This figure shows experiments with a single-pulse state at $\mu = 0.5$ and $L = 40$. This equilibrium is well to the right of the threshold of radiative instability in Fig. 5, at which point, in fact, the state is actually supercritically unstable. As is evident from Fig. 2(a), this single-pulse state possesses a total of five pairs of unstable, complex eigenvalues. Of these, the r_3 and r_4 modes are dominant. The two calculations shown in the figure begin with slightly different initial perturbations off the unstable equilibrium. In panel (a), the mode r_3 emerges initially with largest amplitude. It grows with little influence from the original pulse, which survives after the creation of three new pulses. In panel (b), the mode r_4 emerges first, and the final state consists of only three pulses. Though the final state has some dependence on the

initial condition and dominating instabilities, the pathway taken to the final configuration is complicated. That the lower-order mode creates the more pulses illustrates that one cannot straightforwardly predict the outcome of violent growth of radiation modes.

The pulse-creation events of Fig. 11 illustrate the outcome of strong radiative instabilities irrespective of whether they are supercritical or subcritical at threshold. These experiments are also similar to situations in which the system relaxes to a pulse train from some very different initial condition. The final number of pulses can be bounded above by the occurrence of separation-limiting instabilities, and from below by constraints imposed by the finite width of a pulse. For example, for the domain size $L = 40$, the single and double-pulse states are both unstable; the domain cannot contain more than six pulses. Secondary instabilities complicate the issue even further (the six-pulse state permitted in a domain of size 40 is unstable).

Roughly, we can estimate the number of pulses in the final train as follows. The unbounded vacuum state has an unstable continuum of eigenvalues. That continuum peaks at modes whose spatial scales (wavelengths) lie in the vicinity of $2\sqrt{2}\pi \simeq 9$. This suggests that the maximally growing instability, which can be plausibly taken to yield a typical pulse separation, generates a pulse train with characteristic spacing, $\overline{\Delta} = 9$. In fact, this is an underestimate of the pulse separation since there is clearly a scale difference between infinitesimal disturbances and pulse equilibria (Fig. 1). For values of μ near 0.5, numerical experimentation indicates that a more accurate estimate of the typical pulse separation is just over 10 (this estimate depends on the amount of dispersion). Therefore, pulse creation from the vacuum should typically produce trains with rather short spacing (see Fig. 4). Creation from unstable pulse states produces trains with somewhat larger spacing.

B. Saturated supercritical solutions

In addition to ascending to larger period, the finite-amplitude supercritical radiative branches also tend to wind back and forth as we vary L. An interesting feature of the $\mu = 0.4$ solution branch, a portion of which is pictured in more detail in Fig. 9(f), is that it loses stability within the region marked by stars. In the original infinite-dimensional phase space corresponding to the spatial variable x, the radiative solutions lie on invariant

tori characterized by the frequencies, $2\pi/L$ and ω (the frequency of the nonlinear radiation mode). In a suitable Galilean frame, these tori collapse down to limit cycles. Along the magnified branch of the radiative solution, this limit cycle loses stability in a (supercritical) period-doubling bifurcation. If we increase the domain size further, there is a second such bifurcation and a stable period-four orbit emerges. This progression is displayed as a sequence of phase portraits in Fig. 12(a). These portraits are generated by plotting the solution at one point in the moving frame against the solution at another point, distance $L/7$ away.

Figure 12(a) illustrates the inception of a cascade of period-doubling bifurcations. This generates what we interpret to be strange attractors at larger L; samples are presented in Fig. 12(b). An important feature of these irregular states is that chaos is barely discernible; space-time surface plots of short-interval pieces of the solution are superficially regular. Only on sufficiently long timescales can we discern the temporal irregularity (Fig. 13).

In larger domains ($L \gtrsim 20$), it becomes difficult to find any strange attractors related to those shown in Fig. 12(b). From various initial conditions, the system hovers near what looks to be the strange set for a time, but then rapidly departs and converges to the stable, periodic, radiative branch at lower amplitude. This probably results from the collision of the set with a fixed point which destroys its asymptotic stability (a so-called "crisis"), but we have not explored such a possibility. In any case, towards larger values of L, the set regains attractiveness and inverse period doubles back to the original radiative branch (Fig. 12(c)).

The behavior of the supercritical radiation branch is very much like beginning of Shil'nikov's route to homoclinicity.[17] That route is characterized by a periodic orbit which winds through an infinite number of saddle-node bifurcations into a homoclinic orbit. In addition, along each stable branch, period-doubling bifurcations begin cascades that generate infinitely many, unstable periodic orbits. In paper I we found that, as orbits within a three-dimensional dynamical system, the steady pulse trains are nearly homoclinic solutions that also follow the bifurcation pathways predicted by Shil'nikov theory. It is rather amusing that both the steady trains and their time-dependent radiative dynamics have the Shil'nikov flavor. Although calculations with single or double-pulse states may be largely irrelevant, this raises the question of whether spatially extensive pulse trains can be irregular in both space and time as a result of mechanisms that can both be described by homoclinic theory.

VI. DYNAMICS AT SMALL DISPERSION

A. Inertial-mode instability

Radiative instability at larger values of μ appears to create temporally chaotic states. These constitute solutions that occupy a very small window of the total parameter space and their basins of attraction are small. This fragility of complexity is apparently a common hallmark of homoclinic chaos.[3,2] At smaller values of μ, temporally complicated solutions arise through different transition mechanisms, and are more common and persistent. In this section we present two examples for which solutions bifurcate to temporal complexity. These examples are meant only as illustration of the wealth of different behavior present in the PDE (1), and are not meant to give a complete picture of the bifurcation sequences possible.

In Fig. 4, we drew the threshold of instability of the inertial mode. This is a localized mode that describes overstable compressional oscillations of the train of pulses. Beyond the threshold of overstability, at $L = 19$, if we track the solution to smaller μ, the amplitude of the inertial mode saturates supercritically. Once again, in an appropriately moving frame, the finite-amplitude solution is seen as a limit cycle. It loses stability first in a symmetry-breaking bifurcation which destabilizes the purely antisymmetrical oscillation of the two pulses. Thereafter, symmetry-broken oscillations are stable until a period-doubling bifurcation. Once again, this second bifurcation sparks a cascade. In Fig. 14 we show period one, two and four orbits and a ribbon-like, (presumably) strange attractor. This figure portrays the solutions as phase portraits projected onto the $\Delta - \dot{\Delta}$ plane (because of symmetry breaking only the first of the limit cycles has the invariance, $\Delta \to L - \Delta$). Details of the strange object are revealed in Fig. 15, which shows a plot of one maximal spacing against the following maxima. In appearance, this function looks like a typical attractor of the Hénon map,[21] $x' = y$ and $y' = 1 - ay^2 + bx$. It is superficially double-valued, but appears fractal in detail. Although it is not strictly a one-dimensional map, we informally refer to the graph of successive maxima in Δ as the maximal spacing map.

The strange object develops further as we lower μ. The pulse positions over many characteristic periods are displayed in Fig. 16 for four experiments at different dispersion. Just after the period-doubling cascade, the space-time pattern is imperceptibly irregular. Some-

what further beyond the cascade (panel (b)), chaos is more visible, but the pulses preserve their mean positions. By $\mu = 0.07$, new features become evident (panel (c)). These are what one might call "phase jumps." These jumps jar the pulses out of alignment, and lead to sharp dislocations in the space-time pattern. Even more extreme events occur at yet lower μ; the pulses apparently collide and merge, and a new one nucleates (panel (d)).

Figure 17 shows maximal spacing maps for the first three experiments of Fig. 16. In panel (a), the map consists of two pieces. These two pieces correspond to the two distinct attractors arising from the period-doubling cascades of the two symmetry-broken limit cycles (in Fig. 15, only one of the attractors is displayed). Shortly below $\mu = 0.08$, the two attractors expand and intersect, then merge into one (Fig. 17(b)).

In the maximal spacing maps, phase jumps appear as sporadic excursions away from the main body of the attractor (Fig. 17(c)). The *annihilation–nucleation events* seem to be more extreme versions, but because it is no longer possible to identify spacings during the events, we can no longer draw a maximal-spacing map. The mechanism behind the phase jumps and annihilation–nucleation events becomes clearer on plotting phase portraits for the system. Portraits projected onto the $\Delta - \dot{\Delta}$ plane are shown in Fig. 18. After the two asymmetrical attractors merge, the strange object gradually grows and begins to approach the fixed point corresponding to an asymmetrical two-pulse state with spacings of 6.555 and 12.445. (In the phase portraits of Fig. 18, the fixed appears to lie within the strange set, but this is purely an artifact of projection.) When the trajectory nears this fixed point, it becomes attracted towards its stable manifold. Phase jumps occur when the trajectory approaches the fixed point too closely, then rapidly departs from the vicinity of that point in the direction of its unstable manifold.

For some value of μ between 0.07 and 0.0675, the inertial-mode attractor collides with the fixed point. Trajectories can then pass around the stable manifold of this saddle-point. There follows a rapid evolution away from the strange set in the phase space that corresponds to the annihilation–nucleation event. This event is shown in more detail in Fig. 19.

Pulse annihilation–nucleation therefore corresponds to the loss of asymptotic stability of the strange set. The event takes the system on a rapid excursion in phase space, but then the trajectory returns to the neighborhood of the strange set; the metastability of this set then

leads to the intermittent dislocations present in the evolution of the pulse positions. It is an example of *on/off intermittency*,[34] or, more specifically, the *crisis-induced intermittency* of Grebogi, Ott and Yorke.[19]

B. Nearly heteroclinic dynamics

If we decrease μ further, the number of annihilations and nucleations increases over a given time period as the strange set loses further stability. The space-time plot of the solution then takes on a rather erratic appearance (Fig. 20).

At even smaller dispersion, the irregularity of the solution begins to decline once more. In time, the solution acquires the character of a relaxation oscillation between a pair of briefly coherent steady states (Figs. 21(a) and (b)). These approximately steady states are two-pulse equilibria, phase shifted from one another by $L/2$. The transition between the two states occurs when an inertial-mode instability amplifies and triggers an annihilation–nucleation event, which generates the new state.

If we take slices through the space-time pattern (in a suitably moving frame), the time traces have a similar character to a train of irregularly spaced kinks or fronts (Figs. 21(c) and (d)). In order to understand the occurrence of states of this kind we display in Figs. 22 various phase portraits of the solution at $\mu = 0$. These portraits reveal that the train of kinks is comprised of almost heteroclinic connections of the two phase-shifted equilibria, a phenomenon encountered previously for the Kuramoto-Sivashinsky equation[9,23] (that is, the PDE (1) with $\mu = 0$). Moreover, the connections spiral both in and out of the fixed points (they are *bi-focal* orbits). For these values of μ and L, the two-pulse equilibrium state has an unstable complex eigenmode (the inertial mode) with eigenvalue $+0.08 \pm 0.4i$. The least decaying modes are a complex pair with eigenvalue $-0.27 \pm 0.46i$. The rates at which the trajectory spirals into and out of the fixed points coincides roughly with these eigenvalues, and so it seems reasonable to suppose that the solution winds out of the unstable manifold of the fixed point, then back in predominantly within the plane spanned by the eigenvectors of the least unstable complex pair.

Like the homoclinic orbits that our basic pulses correspond to, four-dimensional bifocal heteroclinic orbits can be analyzed with Shil'nikov theory.[15] This reduces the problem of

nearly-heteroclinic dynamics to the iteration of a three-dimensional map. Provided the system is sufficiently dissipative, the map can be replaced by an approximation of lower dimension. In our case, the orbits in phase space are a little more complicated than simple heteroclinic connections; other fixed points appear to influence the trajectory. Moreover, at $\mu = 0$, the system is reversible in time, so the flow in phase space is volume preserving, and it is typically difficult to study such situations with Shil'nikov theory. For these reasons we have not pursued analysis of the heteroclinic patterns in any detail (but see Ref. 9).

At larger values of μ, the quality of the heteroclinic connection is diminished; the interval between events is smaller and the regularity of the space-time pattern is degraded. For a value of μ of about 0.0015, the nearly heteroclinic attractor appears to collide with the unstable steady solution corresponding to the asymmetrical two-pulse state. This leads to intervals of rapid evolution in phase space, during which the trajectory flies away from the nearly-heteroclinic set, but then approaches it once more. As for the phase jumps in the pulse positions at larger μ, this generates intermittent dislocations in the space-time pattern of the solution (see Fig. 23).

C. Radiative states at small μ

An alternative route to temporal complexity arises from tracking radiative instability from its inception to smaller μ. According to Fig. 5, the symmetrical two-pulse equilibrium bifurcates to instability in domains of size $L = 29$ at $\mu \simeq 0.2$. At that point, a supercritical, radiative branch of solutions emerges. This solution branch first loses stability to a modulational or subharmonic mode with an incommensurate frequency. Then the state suffers a symmetry breaking instability. Both bifurcations are supercritical, and we find a doubly periodic, asymmetrical radiative branch.

At $\mu \simeq 0.1308$, this solution apparently ceases to exist as the result of a saddle-node bifurcation. Beyond the bifurcation, there emerges a wealth of temporally intermittent patterns (Fig. 24). The transition to temporal chaos therefore occurs through a mechanism of the Pomeau-Manneville type I variety.[33]

At smaller values of μ, the degree of intermittency declines, and incoherent states become predominant. For $\mu = 0$, evolution from the two-pulse state proceeds as shown in Fig. 25.

This illustrates a sequence in which a radiative instability destroys the initial two-pulse configuration leaving a four-pulse state that undergoes a nearly heteroclinic transition to its $L/2$ phase-shifted relative. The second four-pulse state begins another phase shift, but then loses stability and the system eventually converges into a rather interesting periodic solution containing an almost stationary pulse, and two other, oscillating peaks.

VII. DISCUSSION

A. The relevance of asymptotic theory

In this paper we have studied the dynamics of interacting pulses in a medium whose homogeneous state is unstable. More specifically, we have described the dynamical fate of pulses in relatively small, periodic domains. In such settings, we can crudely catalogue the behavior as follows. For larger values of μ, the system slowly settles into moderately spaced trains. For smaller amounts of dispersion, pulses exhibit temporally complicated motions either through their own interactions, or because of spatially unlocalized instabilities.

In larger domains, we expect initial configurations with a small number of pulses violently to create new ones. This regulates the typical spacings between the pulses of a train. It reflects the most serious failing of the analytical theory we have considered. Simultaneously, however, it also provides its possible savior; the outcome of creation is a train with moderate spacings that can fall within our "accessible range" of dynamics, at least for large μ.

It is quite illuminating to establish the degree of complexity in the solutions of a simple PDE like (1). At the outset, one might have felt that, aside from some interesting transient behavior,[11] steady pulse trains were eventually its only solutions. That feeling has certainly motivated some earlier, analytical studies.[12,13] However, in what we might call the ideal limit, $\mu \to 0$, the system loses all semblance of simplicity in its range of behavior. The asymptotic theory of pulse interaction described in Sec. II is not, therefore, of great generality, a noteworthy point if we are to advance to consider more complicated situations like higher dimension.

We can attempt to improve the asymptotic theory in order to remove its shortcomings. In fact, the need to include radiative instability was the motivation for the analysis of Appendix B, which, unfortunately leads to a rather convoluted formulation. Along a similar vein we

could try to treat inertial-mode dynamics by decomposing the pulse train into well separated pulses and narrowly spaced pairs. The dynamics of the inertial modes can then be accounted for by replacing the pairs by individual entities with internal degrees of freedom, much as one treats the intrinsic degrees of freedom of kinks in nonlinear field theories.[5] The experiments described in Sec. VI suggest that the internal dynamics can be complicated, though possibly reproducible by a low-order dynamical system. It seems difficult, however, to extract an analytical theory of such dynamics. In practice, it may prove simpler to formulate a hybrid scheme in which we evolve the individual pulses under asymptotic, long-range interactions and numerically simulate any close encounters.[39]

In principle, then, we might formulate an improved theory of pulse dynamics, incorporating both radiation and inertial modes. That formulation, however, is complicated and probably not sufficiently general to provide a theory of coherent-structure dynamics. Indeed, in reaction-diffusion systems, bifurcations appear to set fronts into oscillatory and even chaotic motion.[10,8,20,25] These arise through localized effects rather than global radiation-like modes, and may affect even isolated fronts. Thus, such frontal dynamics seems largely to be of a different flavor to the pulse dynamics considered here. The distinction between our thin-film problem and these excitable systems probably has its origin in the absence of vacuum instability from the latter. In kink dynamics in nonlinear field theory there may be a stronger connection since external perturbation and collision can act to excite the otherwise stable radiation modes.[5,14]

B. Multiply peaked pulse equilibria

To return to some further details of the thin-film problem, we have only studied one kind of pulse in the main body of the paper. In earlier investigations[7,22,31] and paper I, it was found that there existed other kinds of steady solitary-wave equilibria. These are specifically pulses which have multiple principal peaks, and for completeness we ought to explore the dynamics associated with them.

The asymptotic theory of Sec. II gives no indication as to the fate of multiply peaked pulses. In fact, since weak pulse interactions are mediated by the exponential tails of the pulses, irrespective of the number of principal peaks intrinsic to them, the asymptotic equa-

tions of motion take an identical form for all of the solitary-wave states. Numerically, however, we find that the multiply peaked pulses all possess inertial-mode instabilities, *i.e.* intrinsic "shape modes" that act to break them apart into groups of singly peaked pulses. The overstabilities seem always to be destructive on single (multiply peaked) pulse states. However, in the presence of other pulses, it may be the case that the inertial mode saturates at finite amplitude. This provides one explanation of the periodic solution found in Sec. VI.C (Fig. 25), which could be viewed as a singly peaked pulse paired with an overstable, doubly peaked pulse. Otherwise there would seem to be no analogue in our current system of the breather solitons that occur in systems like the Sine-Gordon equation.

The intrinsic instability of the multiply peaked pulses implies that it is probably not worth considering them further. This is somewhat unfortunate since these solutions move at sufficiently different speeds to permit fast collisions between the localized objects. Otherwise such events are precluded by the tight speed controls imposed by the dynamical balance making up the solitary-wave envelopes. In Fig. 26 we record a collision between a singly peaked pulse and its doubly peaked relative. It is made somewhat interesting because the event proceeds too quickly for any intrinsic instability to become manifest. The collision (unsurprisingly) breaks apart the doubly peaked pulse, and three of the singly peaked variety emerge, together with an unlocalized disturbance. Subsequently the disturbance excites a radiative instability that nucleates another pulse. In our dissipative system (1), collisions of this kind are the only analogues of the comparatively perfect, soliton collisions. Other equations modelling instabilities on thin films have a richer range of collisional behavior.[6,27,32]

C. A remark on Galilean invariance

We conclude with a remark concerning Galilean invariance. As explained in Appendix A, the additional symmetry associated with this invariance has no effect upon the dynamics of the pulses in leading-order asymptotic theory. This is not to say that Galilean invariance plays a minor role in the general dynamics of pulses in the PDE (1). In fact, its role is critical. The PDE conserves the spatial average,

$$\bar{u}(t) = \int_{-L}^{L} u(x,t)dx. \tag{24}$$

Individually, each pulse has a certain average value, $\overline{H}$, associated with it. Therefore, in order to create a new pulse, which is seemingly the tendency of the PDE over a large regime in its parameter space, we cannot simply add a pulse onto the initial state. In fact, in order to create new pulses we must change the average of the initial state. It is the ability of the system to accelerate into a new Galilean frame (hence modify its average) that permits the nucleation of new, individual pulses. When we break the Galilean invariance, the system can no longer make a Galilean boost to allow pulse creation. Instead, the rapid evolution resulting from violent radiative instability typically generates states that do not take the form of pulse trains. In this respect, then, Galilean invariance is crucial with regard to pulse dynamics in the thin-film equation (1).

Acknowledgments

A large fraction of this work was completed at various sessions of the Geophysical Fluid Dynamics summer school, Woods Hole Oceanographic Institution; we thank the various participants. In particular, we acknowledge many conversations with E. A. Spiegel, L. N. Howard, J. B. Keller and P. J. Morrison.

APPENDIX A: ON GALILEAN INVARIANCE

The PDE (1) possesses two invariances, namely translational and Galilean. In singular perturbation theory, such invariances are typically of primary importance; they provide free parameters with which we use to construct asymptotic solutions.

Translational invariance allows us to centre solutions on the x-axis wherever we choose; if $u(x,t)$ is a solution, so must be $u(x-x_0,t)$, where x_0 is constant. In the main text we employ this freedom to distribute a set of localized solutions, $H(x-ct-\xi_k)$, along the $x-$axis to construct an approximate pulse train. For well separated pulses, in the vicinity of any particular one, the ansatz, $u \sim H(x-ct-\xi_k)$, is accurate to order ε, and so there are ξ_k free parameters. The arbitrariness involved in locating the pulses relative to one another is removed by singular perturbation methods.

Galilean invariance allows us to add a boost, V, to a solution whilst simultaneously moving into a frame moving with speed V. Thus we also have the solution $u(x-Vt,t)+V$. In principle, the presence of this extra degree of freedom should force us to permit another parameter (namely V), to depend weakly on time and fix it via singular perturbation theory.

In the case of a single pulse we are therefore led to study a solution of the form, $H(x-ct-\xi_k-V_kt)+V_k$, with ξ_k and V_k dependent upon the slow time, τ. For multiple-pulse solutions we must generalize this ansatz, and the question then arises as to how to treat the individual Galilean boosts of all the pulses. A straightforward generalization of the single-pulse approximation leads us to pose an ansatz,[13]

$$u(x,t) \simeq \sum_{k=1}^{K}[H(x-ct-\xi_k-V_kt)+V_k]. \tag{A1}$$

In the vicinity of the k^{th} pulse, this becomes

$$u(x,t) \sim H(x-ct-\xi_k-V_kt)+\sum_{j=1}^{K}V_j, \tag{A2}$$

which cannot be accurate to order ε unless

$$V_k=\sum_{j=1}^{K}V_j. \tag{A3}$$

This implies that no individual boosts are permitted. Our only option for accounting for Galilean invariance is therefore to uniformly boost the entire set of pulses and fix $V_k = V$. In fact, this must be the case since free parameters are assigned exclusively to localized solutions, but any one boost contributes a constant offset to the solution *everywhere*. Therefore, each individual solution, $H(x - ct - \xi_k - V_k t) + V_k$, cannot be considered as localized unless all of the boosts are identical.

Once we allow for a global Galilean shift of the whole pattern, our ansatz is modified to

$$u(x,t) \simeq \sum_{k=1}^{K} H(x - ct - \xi_k - Vt) + V. \tag{A4}$$

A straightforward calculation (multiplying the $O(\varepsilon)$ terms of the PDE by the null vector 1 and integrating over ξ) then generates the solvability condition $dV/d\tau = 0$. In other words, all effects of Galilean invariance (inertia) become buried at order ε^2. Hence we deal with an overdamped system. The ansatz (A4) was not employed by Elphick *et al.*[13] They introduced a different ansatz like (A1) that permitted individual Galilean shifts with the result that their asymptotic solution generated equations of motion for the positions of the pulses that were of artificially high order.

The effects of Galilean invariance are also discussed by Chang and Demekhin.[6]

APPENDIX B: RADIATIVE PULSE DYNAMICS

Asymptotic theory of pulse dynamics fails, as we have seen, when radiative modes bifurcate to instability (Sec. III). To take some account of this phenomenon, we now modify the singular perturbation theory. Our modification bears some similarity to the analysis of a nonlinear field theory presented in Ref. 14. We consider a situation in which there is a train of pulses whose separations are sufficiently wide to permit a radiation mode to become very weakly damped or even unstable. To represent the radiation mode, we introduce the expression,

$$v(\xi,t) = A\varphi(\xi)e^{i\omega t} + \text{c.c.}, \tag{B1}$$

where A is the modal amplitude, $\varphi(\xi)$ is its spatial eigenfunction and ω its frequency. The slow decay or growth of the mode is accommodated by permitting the amplitude to vary on the long timescale: $A = A(\tau)$.

In order to decide the magnitude of the mode's amplitude, we observe that rapid temporal oscillation cancels linear terms in A over long times. Radiation can therefore only affect the pulses nonlinearly through the term, $\partial_\xi(v^*v)$. In order to bring this term into the evolution equation at $O(\varepsilon)$ for the pulse positions, we must fix the wave field to be $\varepsilon^{1/2}v$.

Our ansatz is now modified to become,

$$u(\xi,t) = \sum_k H_k + \varepsilon^{1/2}v(x,t,\tau) + \varepsilon\mathcal{R}(t,\xi,\tau) + \varepsilon^{3/2}\mathcal{S}(t,\xi,\tau) + O(\varepsilon^2). \tag{B2}$$

In addition, we expand the parameter, μ, about the marginal condition, $\mu \sim \mu_0 + \varepsilon\mu_1$, so that we may introduce a control parameter, μ_1. If we introduce these expansions into the governing PDE (5), and once more asymptotically order the various terms, we find the expression,

$$\sum_k \partial_\xi \left[\left({\partial_\xi}^3 + \mu_0 {\partial_\xi}^2 + \partial_\xi - c \right) H_k + \frac{1}{2}H_k^2 \right] +$$

$$\varepsilon^{1/2}(i\omega + \partial_\xi\mathcal{L})v +$$

$$\varepsilon \left\{ (\partial_t + \partial_\xi\mathcal{L})\mathcal{R} + \sum_k \left[\partial_\tau H_k + \mu_1 {\partial_\xi}^3 H_k + \frac{1}{\varepsilon}\partial_\xi(H_kH_{k+1} + H_kH_{k-1}) \right] + v\partial_\xi v \right\} +$$

$$\varepsilon^{3/2} \left[(\partial_t + \partial_\xi\mathcal{L})\mathcal{S} + \partial_\tau v + \mu_1 {\partial_\xi}^3 v + \partial_\xi(\mathcal{R}v) \right] = O(\varepsilon^2), \tag{B3}$$

where we have used the short-hand notation, $H_k = H(\xi - \xi_k)$, and

$$\mathcal{L} = \partial_\xi{}^3 + \mu_0 \partial_\xi{}^2 + \partial_\xi - c + \sum_k H_k. \tag{B4}$$

The term of the third line of equation (B3) which contains the factor $1/\varepsilon$ arises from the overlap of adjacent pulses. It represents nonlocal pulse interactions and, despite appearances, is order ε.[12]

At leading order we obtain a sum of expressions. Each expression in the sum is just the homoclinic equation, and so the order unity terms vanish automatically. At order $\varepsilon^{1/2}$, we find,

$$(i\omega + \partial_\xi \mathcal{L})\varphi = 0, \tag{B5}$$

which provides the definition of $\varphi(\xi)$; the marginal, oscillatory eigenfunction of the operator, $\partial_\xi \mathcal{L}$.

At order ε, we find an inhomogeneous, linear equation for $\mathcal{R}$ containing terms that depend on the "fast time," t, and terms that do not. To account for both, we divide the correction $\mathcal{R}$ into two pieces,

$$\mathcal{R}(t, \xi, \tau) = R(\xi, \tau) + r(t, \xi, \tau), \tag{B6}$$

and then separate the order ε terms of equation (B.3) into the two relations,

$$\partial_\xi \mathcal{L} R = -\sum_k \left\{ \partial_\tau H_k + \mu_1 \partial_\xi{}^3 H_k + \frac{1}{\varepsilon} \partial_\xi [H_k (H_{k-1} + H_{k+1})] \right\} - |A|^2 \partial_\xi |\varphi|^2 \tag{B7}$$

and

$$(\partial_t + \partial_\xi \mathcal{L}) r = -[A^2 \varphi \partial_\xi \varphi \, e^{2i\omega t} + \text{c.c.}]. \tag{B8}$$

Equation (B7) integrates once to

$$\mathcal{L} R = \sum_k [\dot{\xi}_k H_k - \mu_1 H_k'' - H_k (H_{k-1} + H_{k+1})] - |A|^2 |\varphi|^2. \tag{B9}$$

This equation has a bounded solution for R only provided the inhomogeneous term satisfies the set of solvability conditions,

$$\dot{\xi}_k = \tilde{\mu}_1 + F(\Delta_k) + F(-\Delta_{k+1}) + \alpha_k |A|^2, \tag{B10}$$

with $\tilde{\mu}_1 = \mu_1 I_2 / I_0$ and

$$\alpha_k = \frac{\langle |\varphi|^2, N_k \rangle}{\langle H_k, N_k \rangle}, \tag{B11}$$

where

$$\langle f, g \rangle = \int_{-\infty}^{\infty} f(\xi) g(\xi) d\xi. \tag{B12}$$

Enforcing this condition amounts to determining the free parameters appearing in the leading-order solution. In the absence of the radiation mode, $A = 0$, and equation (B10) reduces to the usual equation of motion for the position of the pulse, given by equation (10).

The second $O(\varepsilon)$ relation, (B8), can, in general, be straightforwardly integrated to give the solution,

$$r = A^2 \psi(\xi) e^{2i\omega t} + A_2(\tau) \varphi(\xi) e^{i\omega t} + \text{c.c.}, \tag{B13}$$

where $\psi(\xi)$ is the spatial dependence of the particular solution and the term proportional to A_2 is the homogeneous solution which we will not actually use.

The terms of equation (B3) of order $\varepsilon^{3/2}$ can be written in the form,

$$(\partial_t - \partial_\xi \mathcal{L}) \mathcal{S} = -\{\partial_\tau (A\varphi) + [\mu_1 \partial_\xi{}^3 \varphi + \partial_\xi (R\varphi)] A + \partial_\xi (\psi \varphi^*) |A|^2 A\} e^{i\omega t} + \text{c.c.} + (\text{other terms}), \tag{B14}$$

where by "other terms" we mean those that are either independent of t, or are harmonics of $\exp(i\omega t)$. In (B14), we have omitted a term proportional to $\partial_\tau \omega$, which can be shown to vanish. Because the eigenfunction depends upon τ only through the implicit dependence on the pulse positions, we can further write,

$$\partial_\tau \varphi = \sum_{k=1}^{K} \frac{\partial \varphi}{\partial \xi_k} \dot{\xi}_k. \tag{B15}$$

In order to derive a bounded solution for $\mathcal{S}$, we must again enforce a solvability condition by multiplying by $\varphi^\dagger$, the eigenfunction of the operator $\mathcal{L}^\dagger$ that is adjoint to φ, and integrating. This yields an equation for the amplitude of the radiation mode,

$$\partial_\tau A + \sum_{k=1}^{K} \zeta_k \dot{\xi}_k A = \varpi' A + \rho' |A|^2 A, \tag{B16}$$

which contains coefficients that depend on the pulse positions in a complicated, implicit way. The coefficient ζ_k is given by,

$$\zeta_k = \frac{\langle \partial \varphi / \partial \xi_k, \varphi^\dagger \rangle}{\langle \varphi, \varphi^\dagger \rangle}. \tag{B17}$$

To record the form of ϖ' and ρ', we first split the solution for R into two parts as follows,

$$R = R_0 + |A|^2 R_1. \tag{B18}$$

Hence R_0 is the solution for R without radiation. This makes the dependence of R on $|A|^2$ explicit, and we write

$$\varpi' = -\mu_1 \frac{\left\langle \partial_\xi{}^3 \varphi, \varphi^\dagger \right\rangle}{\langle \varphi, \varphi^\dagger \rangle} - \frac{\left\langle \partial_\xi (R_0 \varphi), \varphi^\dagger \right\rangle}{\langle \varphi, \varphi^\dagger \rangle} \tag{B19}$$

and

$$\rho' = -\frac{\left\langle \partial_\xi (\psi \varphi^*) + \partial_\xi (R_1 \varphi), \varphi^\dagger \right\rangle}{\langle \varphi, \varphi^\dagger \rangle}. \tag{B20}$$

Equation (B16) can be reduced to a form that resembles a conventional Landau equation for A, by introducing the expressions (B10) for $\dot{\xi}_k$. This gives,

$$\partial_\tau A = \varpi A + \rho |A|^2 A, \tag{B21}$$

with

$$\rho = \rho' - \sum_{k=1}^{K} \alpha_k \zeta_k \qquad \text{and} \qquad \varpi = \varpi' - \sum_{k=1}^{K} [F(\Delta_k) + F(-\Delta_{k+1})] \zeta_k. \tag{B22}$$

In order to evolve the pulses and radiation using these equations, we would need to solve an eigenvalue problem together with its adjoint, and calculate ψ at each step. This reveals the equations to be largely impractical, except in some less general, simpler situations. One such case, is when the underlying pulse train is a single-pulse state in a domain of size L. Equation (B10) then becomes,

$$\dot{\xi}_1 = c_1 + \tilde{\mu}_1 + \alpha_1 |A|^2, \tag{B23}$$

where $c_1 = F(L) + F(-L)$. If we solve (B5) and write the solution as $\varphi(\xi - \xi_1)$, we find, $\partial\varphi/\partial\xi_k = -\partial_\xi \varphi$. Every coefficient then becomes independent of τ. Equation (B22) constitutes a standard Landau equation, and (B23) determines the change to the speed of the pulse train as a function of the amplitude of the radiation mode. Furthermore, the periodic, bifurcated solution branch is given by,

$$|A|^2 = -\text{Re}\,(\varpi)/\text{Re}\,(\rho), \tag{B24}$$

which is quoted in Sec. V.

REFERENCES

[1]A. Arneodo, P.H. Coullet, E.A. Spiegel and C. Tresser, Asymptotic chaos, Physica D **14**, 327-347 (1985b).

[2]N.J. Balmforth, Solitary waves and homoclinic orbits, Ann. Rev. Fluid Mech. **27**, 335-373 (1993).

[3]N.J. Balmforth, G.R. Ierley and E.A. Spiegel, Chaotic pulse trains, SIAM J. App. Math. **54**, 1291-1334 (1993).

[4]D.J. Benney, Long waves on liquid films, J. Mathematics and Physics **45**, 150-155 (1966).

[5]D. K. Campbell, M. Peyrard and P. Sodano, Kink-antikink interactions in the double sine-Gordon equation, Physica D **19**, 165-205 (1994).

[6]H.-C. Chang and E.A. Demekhin, Solitary wave formation and dynamics on falling films, Adv. Mech. (1994), to appear.

[7]H.-C. Chang, E.A. Demekhim and D.I. Kopelevich, Laminarizing effects of dispersion in an active-dissipative nonlinear medium, Physica D **63**, 299-320 (1993).

[8]R.J. Deissler and H.R. Brand, Periodic, quasiperiodic and chaotic localized solutions of the quintic complex Ginzburg-Landau equation, Phys. Rev. Lett. **72**, 478-481 (1994).

[9]Y.A. Demekhin, G.Y. Tokarev and V.Ya. Shkadov, Hierarchy of bifurcations of space-time structures in a nonlinear model of active-dissipative media, Physica D **52**, 338-361 (1991).

[10]J. Elezgaray and A. Arneodo, Modelling reaction-diffusion pattern formation in the Couette flow reactor, J. Chem. Phys. **95**, 323-350 (1991).

[11]C. Elphick, E. Meron and E.A. Spiegel, Spatio-temporal complexity in travelling patterns, Phys. Rev. Lett. **61**, 496-499 (1989).

[12]C. Elphick, E. Meron and E.A. Spiegel, Patterns of propagating pulses, SIAM J. Applied Math. **50**, 490-503 (1990).

[13]C. Elphick, G.R. Ierley, O. Regev and E.A. Spiegel, Interacting localized structures with Galilean invariance, Phys. Rev. A **44**, 1110-1122 (1991).

[14]Z. Fei, V.V. Konotop, M. Peyrard and L. Vásquez, Kink dynamics in the periodically modulated ϕ^4 model, Phys. Rev. A. **48**, 548-554 (1993).

[15]A.C. Fowler and C.T. Sparrow, Bifocal homoclinic orbits in four dimensions, Nonlinearity **4**, 1159-1182 (1991).

[16]J.A. Glazier and P. Kolodner, Interactions of nonlinear pulses in convection in binary fluids, Phys. Rev. A. **43**, 4269-4280 (1991).

[17]P. Glendinning and C.T. Sparrow, Local and global behavior near homoclinic orbits, J. Stat. Phys. **35**, 645-696 (1984).

[18]K.A. Gorshkov and L.A. Ostrovsky, Interactions of solitons in non-integrable systems: direct perturbation method and applications, Physica D **3**, 424-438 (1981).

[19]C. Grebogi, E. Ott and J.A. Yorke, Super persistent chaotic transients, Ergod. Theor. Dyn. Sys. **5**, 341-353 (1985).

[20]A. Hagberg and E. Meron, Pattern formation in non-gradient reaction-diffusion systems: the effects of front bifurcations, Nonlinearity **7**, 805-836 (1994).

[21]M. Hénon, A two-dimensional mapping with a strange attractor, Comm. Math. Phys. **50**, 69-77 (1976).

[22]A.P. Hooper and R. Grimshaw, Travelling wave solutions of the Kuramoto-Sivashinsky equation, Wave Motion **10**, 405-420 (1988).

[23]J.H. Hyman, B. Nicolenko and S. Zaleski, Order and complexity in the Kuramoto-Sivashinsky model of weakly turbulent interfaces, Physica D **23**, 265-292 (1986).

[24]G.R. Ierley, B. Spencer and R. Worthing. Spectral methods in time for a class of parabolic partial differential equations, J. Comp. Phys. **102**, 88-97 (1992).

[25]T. Ikeda and M. Mimura, An interfacial approach to regional segregation of two competing species mediated by a predator, J. Math. Biol. **31**, 215-240 (1993).

[26]B. Janiaud, A. Pumir, D. Bensimon, V. Croquette, H. Richter and L. Kramer, The Eckhaus instability for travelling waves, Physica D **55**, 269-286 (1992).

[27]S. Kalliadasis and H.-C. Chang, Drop formation during coating of vertical fibres, J. Fluid Mech. **261**, 135-168 (1994).

[28]T. Kawahara and S. Toh, Pulse interactions in an unstable dissipative-dispersive nonlinear system, Phys. Fluids **31**, 2103-2111 (1987).

[29]K. Kawasaki and T. Ohta, Kink dynamics in one-dimensional nonlinear systems, Physica **116A**, 573-593 (1982).

[30]J.P. Keener and D.W. McLaughlin DW, Solitons under perturbations, Phys. Rev. A. **16**, 777-790 (1977).

[31]P. Kent and J. Elgin, Travelling-wave solutions of the Kuramoto-Sivashinsky equation: period-multiplying bifurcations, Nonlinearity **4**, 899-920 (1992).

[32]V.I. Kerchman and A.L. Frenkel, Interactions of coherent structures in a film flow: simulations of a highly nonlinear evolution equation, Theoret. Comp. Fluid Dyn. **6**, 235-254 (1994).

[33]P. Manneville and Y. Pomeau, Different ways to turbulence in dissipative dynamical systems, Physica D **1**, 219-226 (1980).

[34]N. Platt, E.A. Spiegel and C. Tresser, On-off intermittency: a mechanism for bursting, Phys. Rev. Lett. **70**, 279-282 (1993).

[35]L.P. Shil'nikov, A case of the existence of a countable number of periodic motions, Soc. Math. Dokl. **6**, 163-166 (1965).

[36]L.P. Shil'nikov, A contribution to the problem of the structure of an extended neightborhood of a rough equilibrium state of saddle-focus type, Math. USSR Sbornik **10**, 91-102 (1970).

[37]S. Toh and T. Kawahara, On the stability of soliton-like pulses in a nonlinear dispersive system with instability and dissipation, J. Phys. Soc. Japan. **54**, 1257-1269 (1985).

[38]C. Tresser, About some theorems of Shil'nikov, Ann. Inst. H. Poincaré **40**, 441-461 (1984).

[39]M.J. Ward, Metastable patterns, layer collapses, and coarsening for a one-dimensional Ginzburg-Landau equation, Stud. App. Math. **91**, 51-93 (1994).

[40]R. Worthing, "On aspects of Benney's equation," in Proceedings of the summer school, *Geophysical Fluid Dynamics*, WHOI 94-12, ed. R. Salmon (Woods Hole Oceanographic Institution, 1993), pp. 257-265.

FIGURE CAPTIONS

FIG. 1. Emergence of periodic pulse trains. Shown is a sequence of profiles of periodic solutions at $\mu = 0.5$ for several values of L (two periods are shown for each).

FIG. 2. Stability properties of single-pulse states. Panel (a) shows the low-order part of the eigenvalue spectrum. Panel (b) shows the real part of the eigenvalues as a function of domain size. Panel (c) illustrates the eigenfunctions of the lowest-order modes. (Modes have been labelled according to the classification scheme outlined in the text.)

FIG. 3. Stability of double-pulse states. Panel (a) shows the low-order part of the eigenvalue spectrum. Panel (b) shows growth rates as functions of domain size; panel (c) is a magnification of part of (b) in which the lattice mode's eigenvalue, calculated according to asymptotic theory, is also plotted as the continuous curve. Panel (d) illustrates the eigenfunctions of the lowest-order modes. (Modes have been labelled according to the classification scheme outlined in the text. Note that the asymptotic eigenvalues are plotted in the original, unscaled time units, not on the $\tau-$scale.)

FIG. 4. Regime diagram for the symmetrical double-pulse states. The region containing equilibria with an unstable inertial mode is labeled by UIM.

FIG. 5. Adjustments between two-pulse equilibria for $\mu = 0.7$ and $L = 28$. Four cases are shown (two with dotted, two with dashed lines). The initial conditions are the unstable equilibrium, $\Delta_1 = 11.6$, with slight perturbations added (the experiments portrayed by dashed lines have initial perturbations to the pulse shapes of order 10^{-3}, those with dotted lines, perturbations of order 10^{-2}). Two conditions relax to the symmetrical $\Delta_1 = \Delta_2 = 14$ state, and the others decay to the state with $\Delta_1 = 9.6$. The complementary asymptotic calculations are also shown (solid lines).

The equilibria have eigenvalues,

Δ_1	η_{num}	η_{asy}
11.58	$+0.0121$	$+0.0126$
14.00	-0.00489	-0.00470
9.51	-0.144	-0.0618

where η_{num} and η_{asy} are the numerical and asymptotic estimates. In the third case there is also a less strongly decaying complex mode with eigenvalue $-0.061 \pm 0.57i$.

FIG. 6. Adjustments between two-pulse equilibria for $\mu = 0.4$ and $L = 28$. Two experiments are shown with dotted lines. These relax from the state with $\Delta_1 = 11.6$ and $\Delta_2 = 16.4$, to either the symmetrical, $\Delta_1 = \Delta_2 = 14$ state, or the periodic steady solution with $\Delta_1 = 9.6$ and $\Delta_2 = 18.4$. Asymptotic calculations are also plotted (solid lines). The equilibria have eigenvalues,

Δ_1	η_{num}	η_{asy}
11.70	$+0.0348$	$+0.0410$
14.00	-0.0256	-0.0221
9.50	$-0.0398 \pm 0.445i$	-0.159

FIG. 7. An adjustment near the border of radiative instability. Shown is evolution from near the unstable symmetrical state with $\Delta_1 = \Delta_2 = 16.88$ (dotted line) and an asymptotic prediction (solid line). The unstable state has eigenvalues, $\eta_{\text{num}} = +0.00309$ and $\eta_{\text{asy}} = +0.00271$. The nearly neutral radiation mode has an eigenvalue with real part -2×10^{-4}.

FIG. 8. The cubic coefficient, ρ, as a function of μ for single-pulse states.

FIG. 9. Finite-amplitude, radiative solution branches as functions of domain size for various values of μ. The figure presents the bifurcation curve in (a) amplitude, $\mathcal{A}$, defined by equation (5.7), and (b) period. Curves are labelled according to the value of μ. Panels (c), (d) and (e) are space-time surface plots of the solution, over two temporal periods at the points marked in panel (a) for $\mu = 0.4$. They are shown in suitably moving reference frames to bring out their structure. Panel (f) shows a detail of the $\mu = 0.4$ solution branch. The stars delimit the stability of the branch. The vertical, dotted lines indicate the locations of the experiments that develop into

the limit cycles and strange objects displayed as phase portraits in Fig. 12. Stable parts of the branch are drawn as continuous curves, unstable ones as dashed curves.

FIG. 10. Evolution of a subcritical radiative instability at $\mu = 0.8$ and $L = 20.5$. Panel (a) shows a contour plot of the solution. Panel (b) shows the world-lines of the principle peaks (defined to be peaks with amplitudes in excess of 0.7 times the global maximum of $u(x,t)$).

FIG. 11. Evolution of radiative instabilities at $\mu = 0.5$ and $L = 40$. Velocity frame with $V = 1.3$. Panels (a) and (c) show space-time surface plots, and (b) and (d) contour plots of the solutions, which more clearly reveal the dominant initial instability.

FIG. 12. Phase portraits projected onto the plane, $[u(x,t), u(y,t)]$, with $y = x + L/7$, in a moving frame. In panel (a), we display the portraits for the period one, two and four solutions. In panel (b), we present the objects we infer to be strange attractors. Panel (c), show portraits before and after the inverse period-doubling cascade (the three portraits are of a strange object, a solution near the period 8 bifurcation point, and a period one solution).

FIG. 13. In panel (a) we plot the variation of the pulse positions in time for the chaotic solution at $L = 20$. A "pulse" in this picture is defined as a peak whose amplitude exceeds 0.7 times the global maximum of $u(x,t)$, which includes the radiation mode over a fraction of its cycle. Panel (b) shows a power spectrum of the solution at a particular point in the moving frame. The frequency of the original periodic solution is labelled as f.

FIG. 14. Phase portraits at $L = 19$ projected onto the $\Delta - \dot{\Delta}$ plane. Shown are period one, two and four limit cycles, and a ribbon-like object we interpret to be a strange attractor. Note that the objects shown, except for the first, do not have the symmetry $\Delta \to L - \Delta$.

FIG. 15. A plot of the maximal spacing values against the following maxima for the strange object shown in Fig. 14. Inset is a picture (inverted) of the Hénon map for $a = 1.7$ and $b = -0.15$.

FIG. 16. Plots of the pulse positions for the apparently chaotic attractors at $\mu = 0.08$, 0.075, 0.07 and 0.0675. In each case, we show the positions relative to a moving frame. In the final panel, pulses annihilate and are created at three instants; this makes the identification of worldlines somewhat ambiguous and so we have plotted the positions as points.

FIG. 17. Graphs of the maximum values of Δ against the following maximal spacings. The data is generated from several experiments and transients have not been suppressed, leading to several outlying points in the pictures. Three panels are shown corresponding to experiments at $\mu = 0.08$, 0.075 and 0.07.

FIG. 18. Phase portraits of the developing strange object projected onto the $\Delta - \dot{\Delta}$ plane. In panel (a) we show portraits at $\mu = 0.08$ and 0.075; panel (b) shows the same at $\mu = 0.07$ and 0.0675. The trajectory of the solution at $\mu = 0.0675$ is continued up to the point for which two pulses apparently collide, and another one nucleates. In panel (b) the fixed point corresponding to the asymmetrical two-pulse state is shown by stars; it appears to lie within the strange set only through projection.

FIG. 19. Space-time plot of an annihilation–nucleation event ($\mu = 0.065$). Panel (a) shows a space-time surfaces plot, and (b) the corresponding contour plot, together with stars indicating the positions of the principal peaks.

FIG. 20. Irregular two-pulse state at $\mu = 0.03$. Panel (a) shows a space-time plot in a moving frame. Panel (b) shows a contour plot together with the positions of the principal peaks. Panel (c) shows a time series of the solution at a particular point in the moving frame, and (d) shows the power spectrum taken from it.

FIG. 21. Solutions at $\mu = 0.005$ and $\mu = 0$. Panel (a) and (b) show space-time surfaces of the solutions in two suitably moving frames. Panel (c) shows time traces extracted from fixed locations, distance $L/4$ apart. Panel (d) shows the intervals between annihilation–nucleation events (defined according to a minimum in the first asymmetrical Fourier coefficient).

FIG. 22. Phase portraits at $\mu = 0$. Two of these portraits, (i) and (ii), were obtained by

plotting the solution at one location in the moving frame against the solution at another point, distance $L/4$ and $L/8$ away. The other portraits are the time series and its temporal derivative of (iii), the first asymmetrical Fourier coefficient, and of (iv), the solution amplitude at a particular point.

FIG. 23. Evolution over longer timescales at $\mu = 0.005$. Plotted are the positions of the pulses against time.

FIG. 24. Intermittent patterns at $\mu = 0.13$, $L = 29$. Shown is a particular contour level of the solution. Roughly, there are three phases: firstly there is a brief two-pulse state; this gives way to a symmetrical radiative state which finally subsides to an asymmetrical, doubly periodic state.

FIG. 25. Evolution from the unstable two-pulse equilibrium at $\mu = 0$, $L = 29$. Two space-time surface plots are shown.

FIG. 26. A collision between a singly peaked pulse and a pulse with two principal peaks. The picture shows a contour plot of the solution with the positions of the principal peaks superimposed.

Figure 1: Development of periodic pulse trains

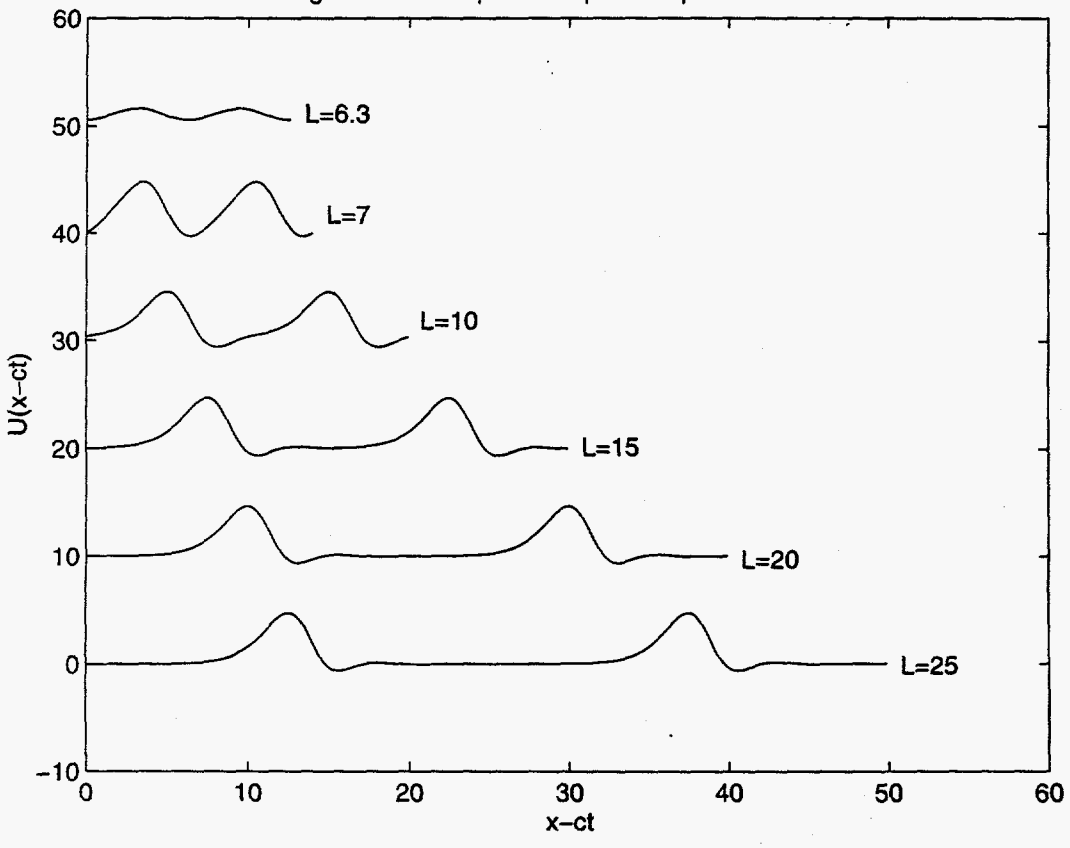

Figure 2

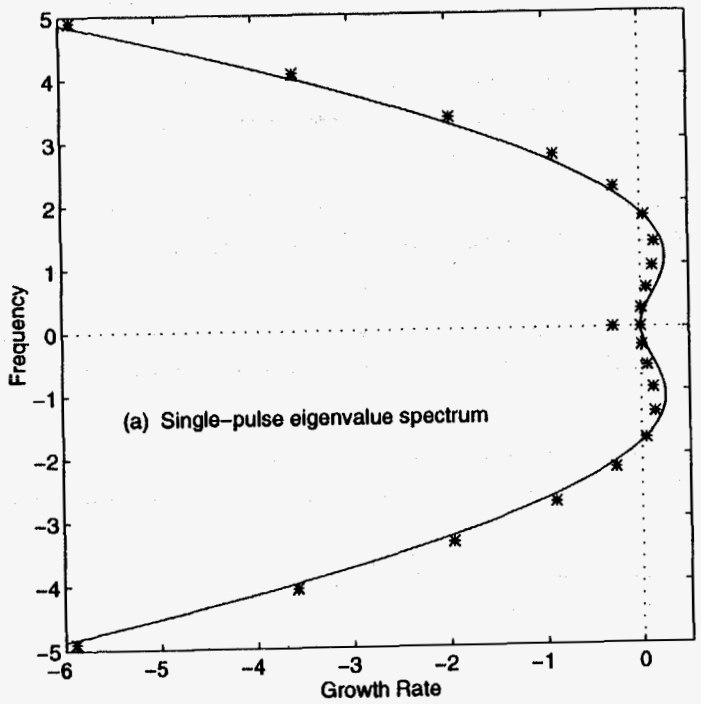
(a) Single−pulse eigenvalue spectrum
Frequency
Growth Rate

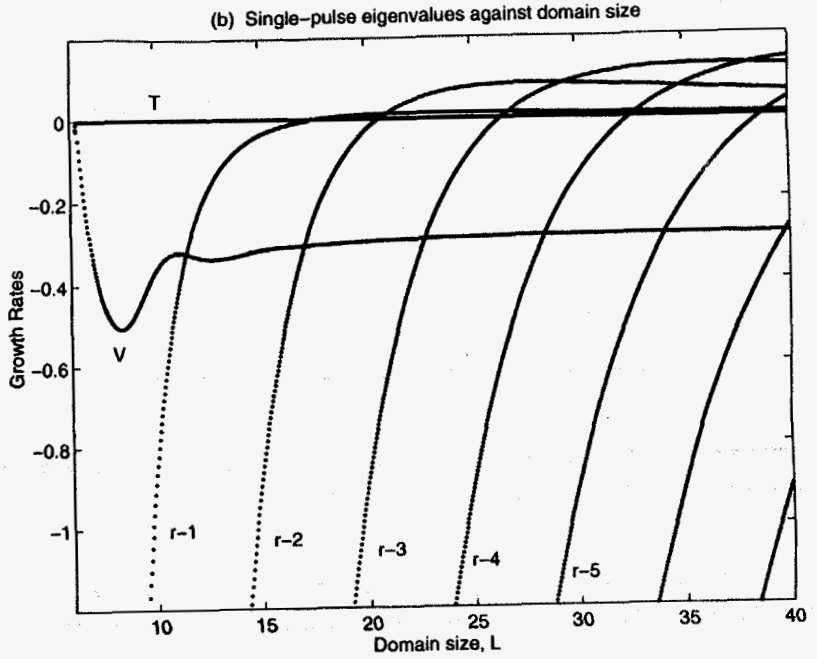
(b) Single−pulse eigenvalues against domain size
T
V
r−1
r−2
r−3
r−4
r−5
Growth Rates
Domain size, L

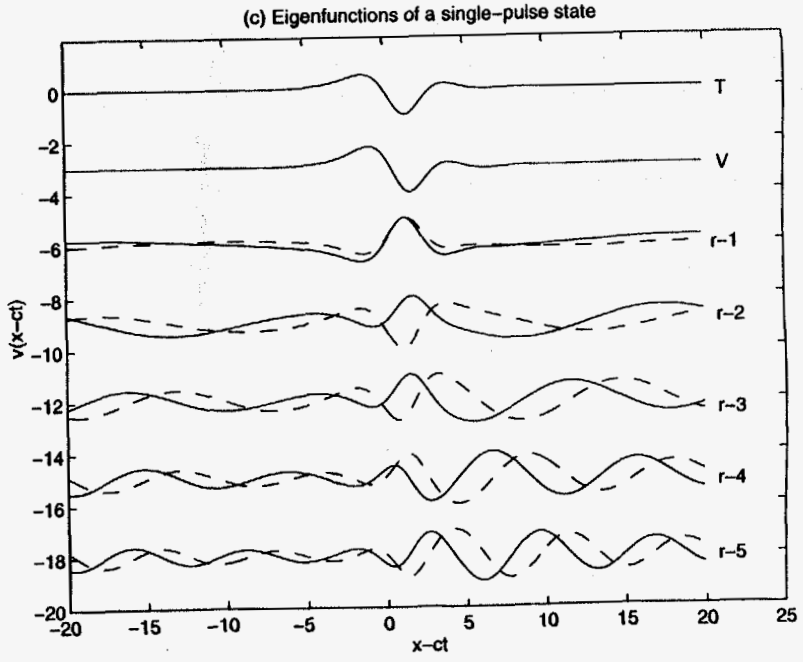
(c) Eigenfunctions of a single−pulse state
T
V
r−1
r−2
r−3
r−4
r−5
v(x−ct)
x−ct

Figure 3

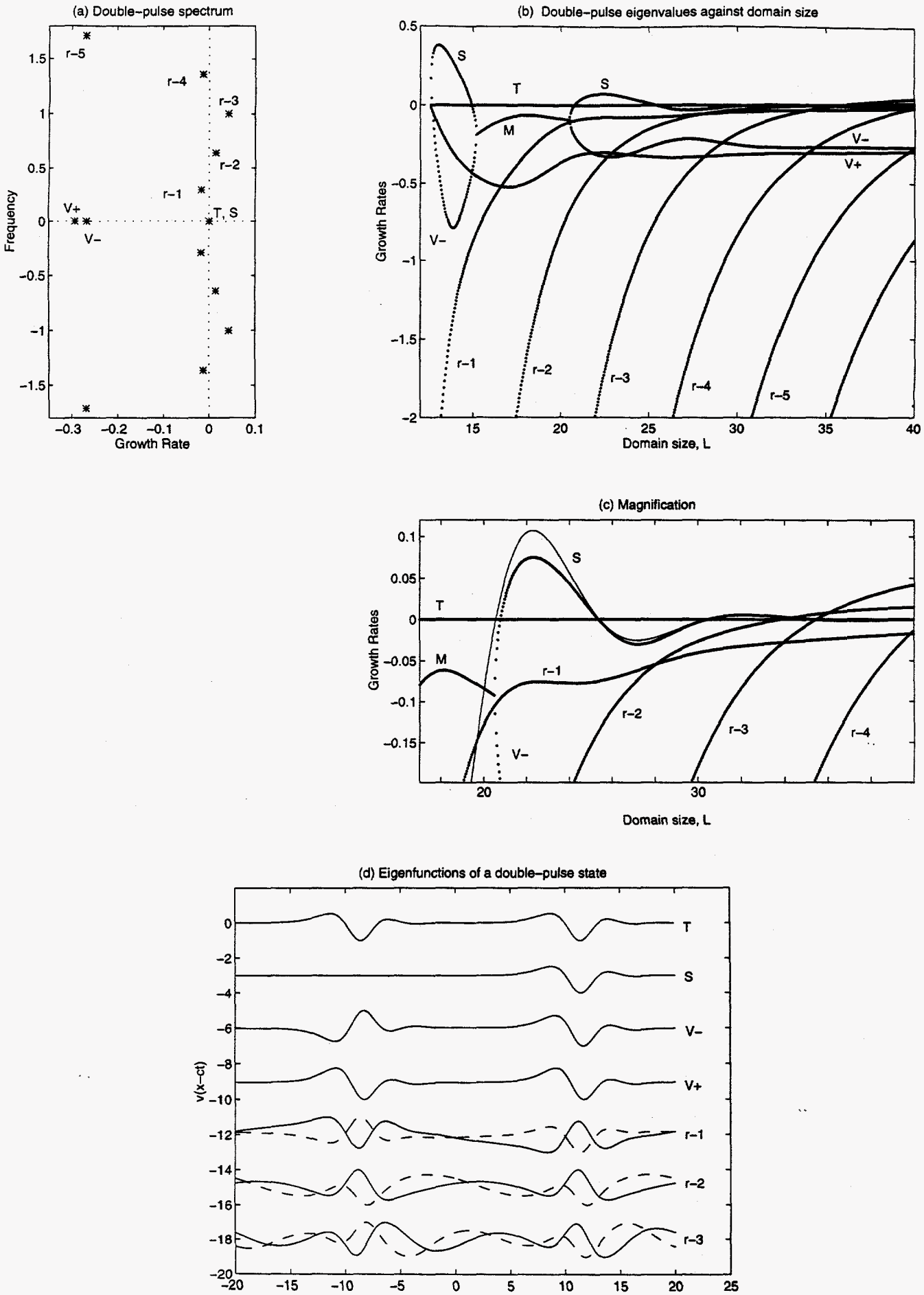
(a) Double-pulse spectrum
r−5
r−4
r−3
r−2
r−1
V+
V−
T, S
Frequency
Growth Rate
(b) Double-pulse eigenvalues against domain size
S
T
S
M
V−
V+
V−
r−1
r−2
r−3
r−4
r−5
Growth Rates
Domain size, L
(c) Magnification
S
T
M
r−1
r−2
r−3
r−4
V−
Growth Rates
Domain size, L
(d) Eigenfunctions of a double-pulse state
T
S
V−
V+
r−1
r−2
r−3
v(x−ct)
x−ct

Figure 4

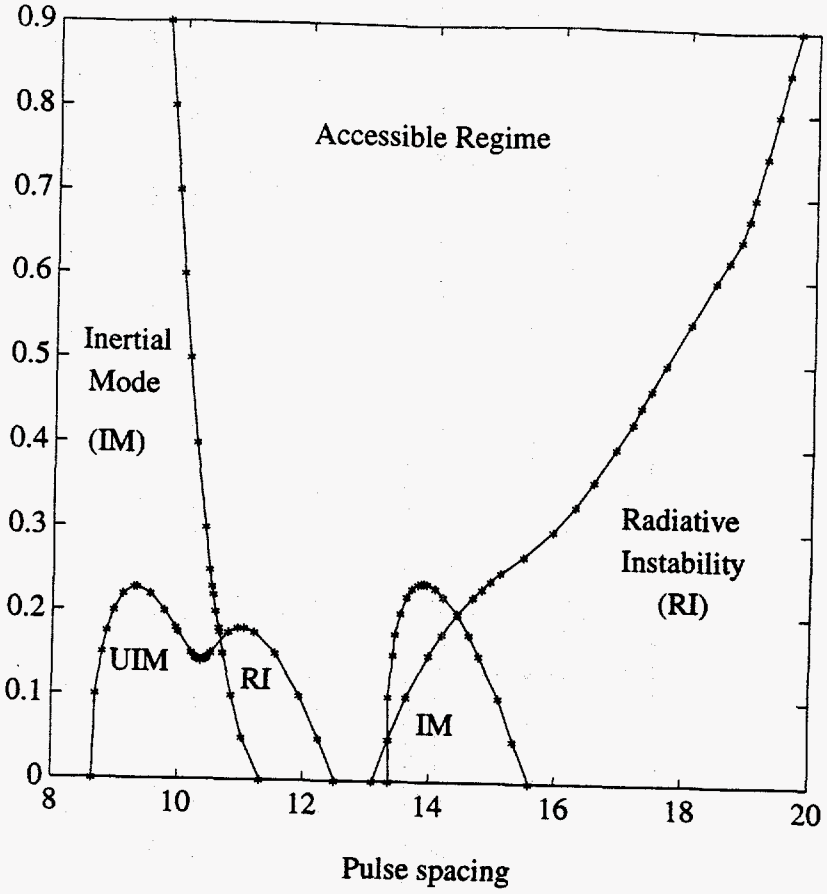
0.9
0.8
0.7
0.6
0.5
0.4
0.3
0.2
0.1
0
8
10
12
14
16
18
20
Accessible Regime
Inertial
Mode
(IM)
UIM
RI
IM
Radiative
Instability
(RI)
Pulse spacing

Figures 5, 6 and 7

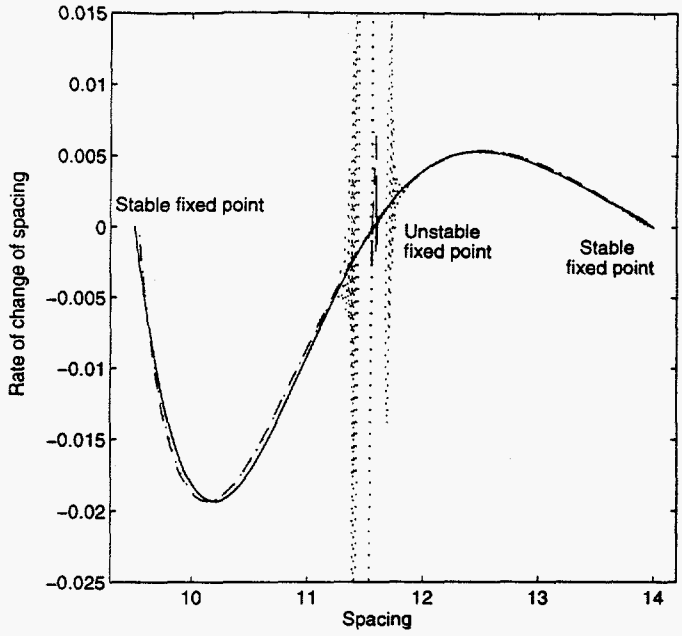

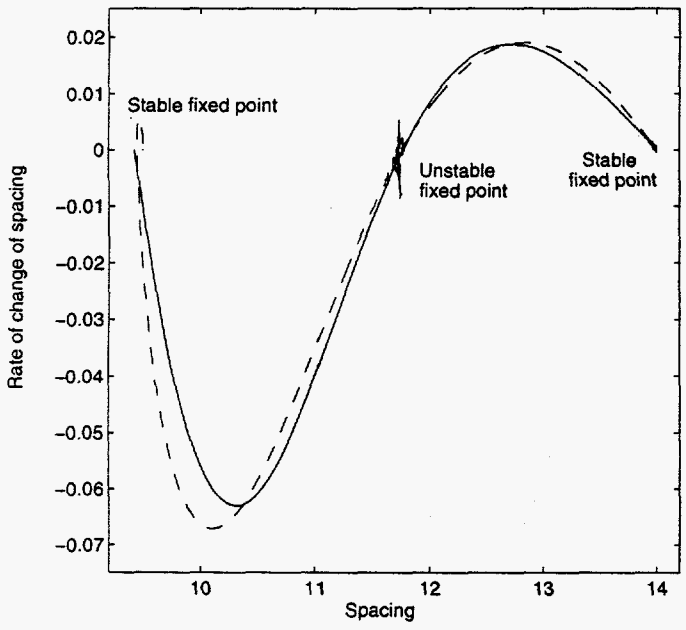

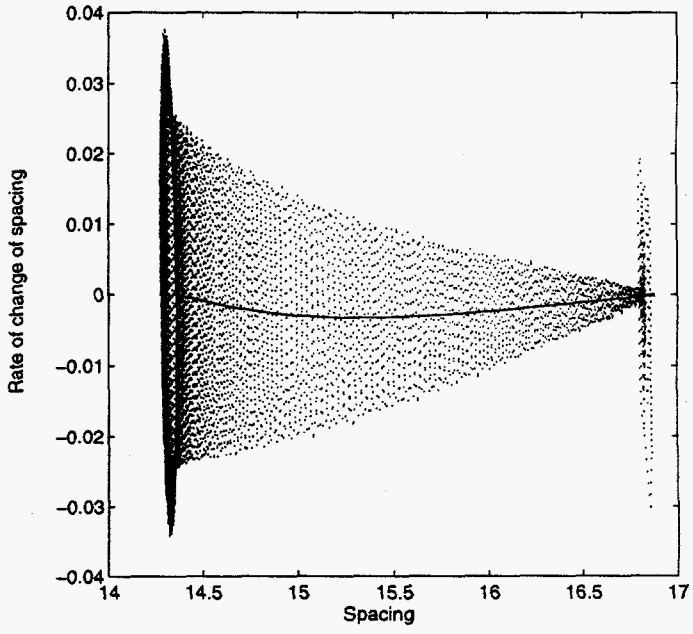

Figure 8: Cubic coefficient, rho

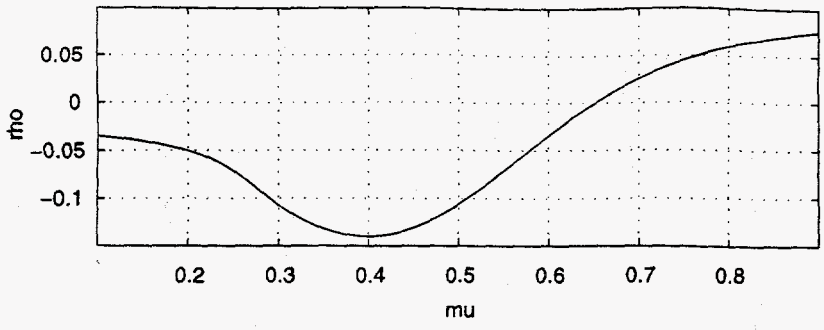

Figure 9(a): Radiative solution branches

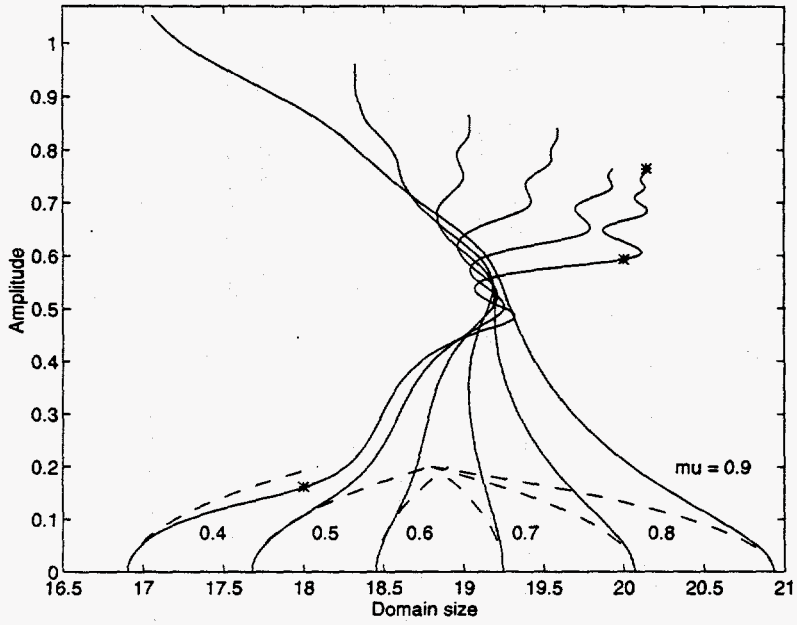

Figure 9(b): Radiative solution branches

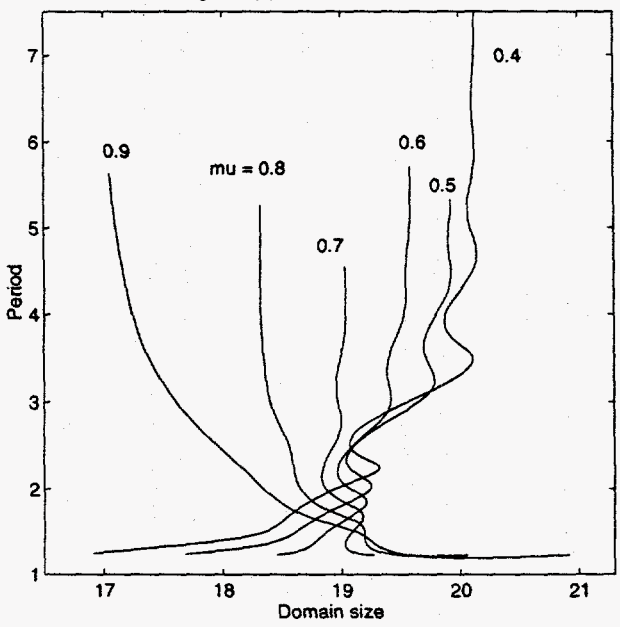

Figure 9

(c) Radiative solution at L=18

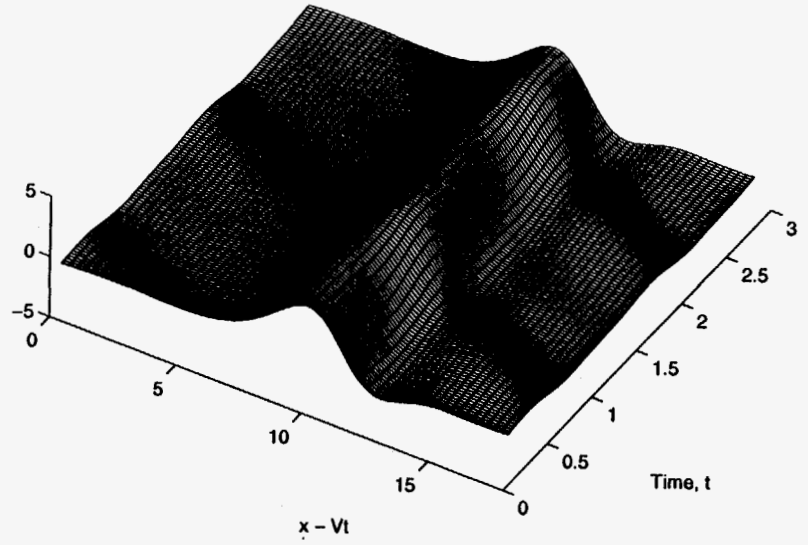

(e) Final periodic radiative solution

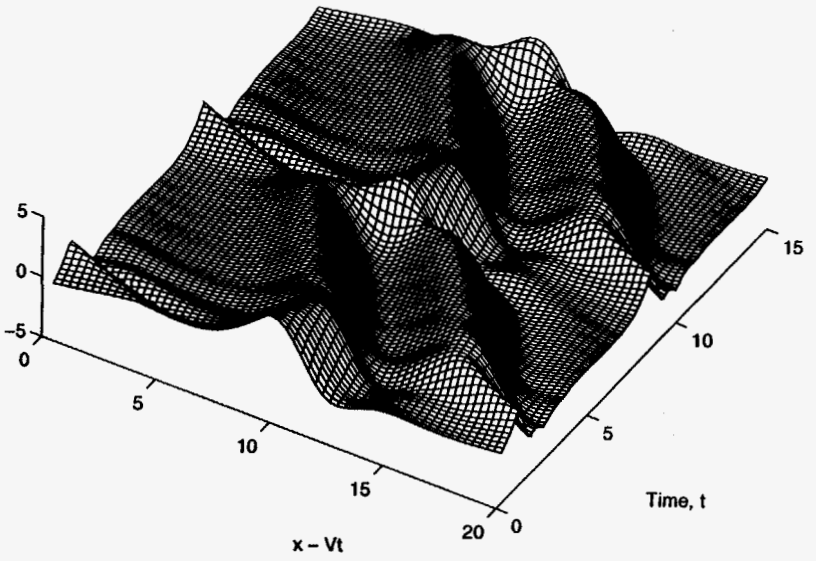

(d) Radiative solution at L=20

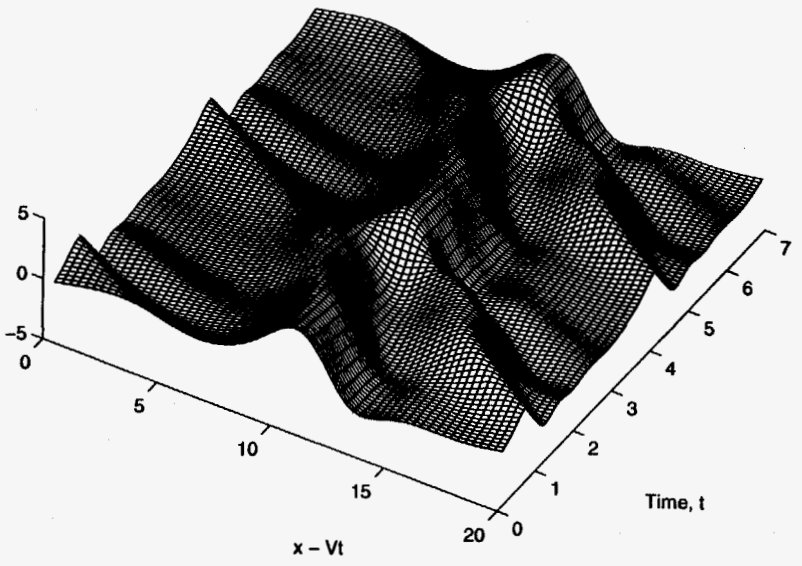

(f) Details of the bifurcated branch at mu=0.4

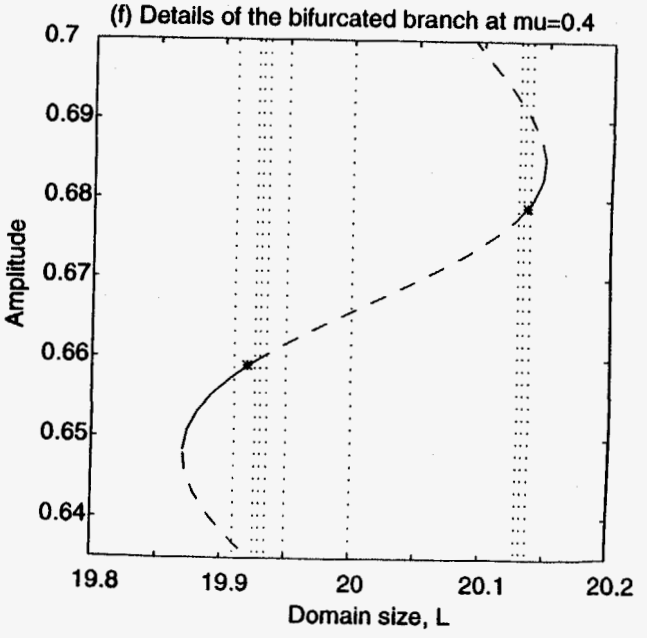

Figure 10

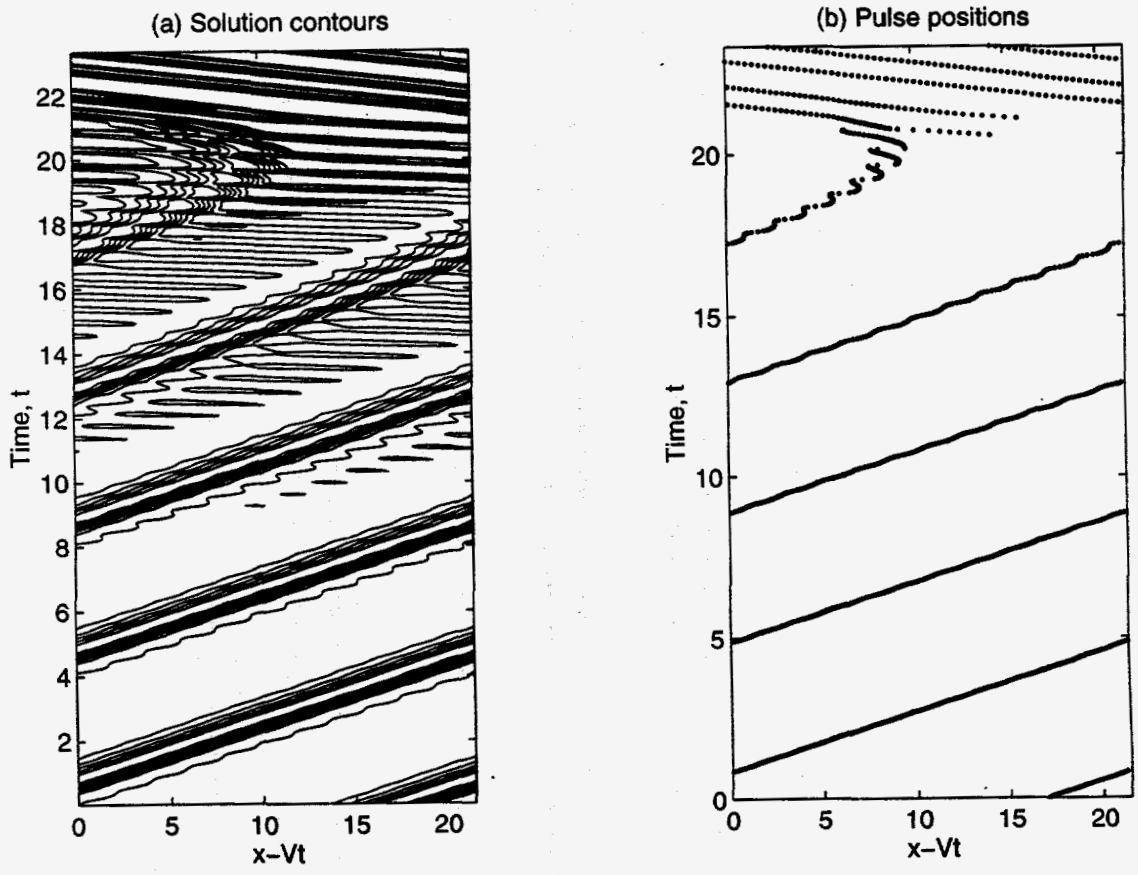

Figure 11

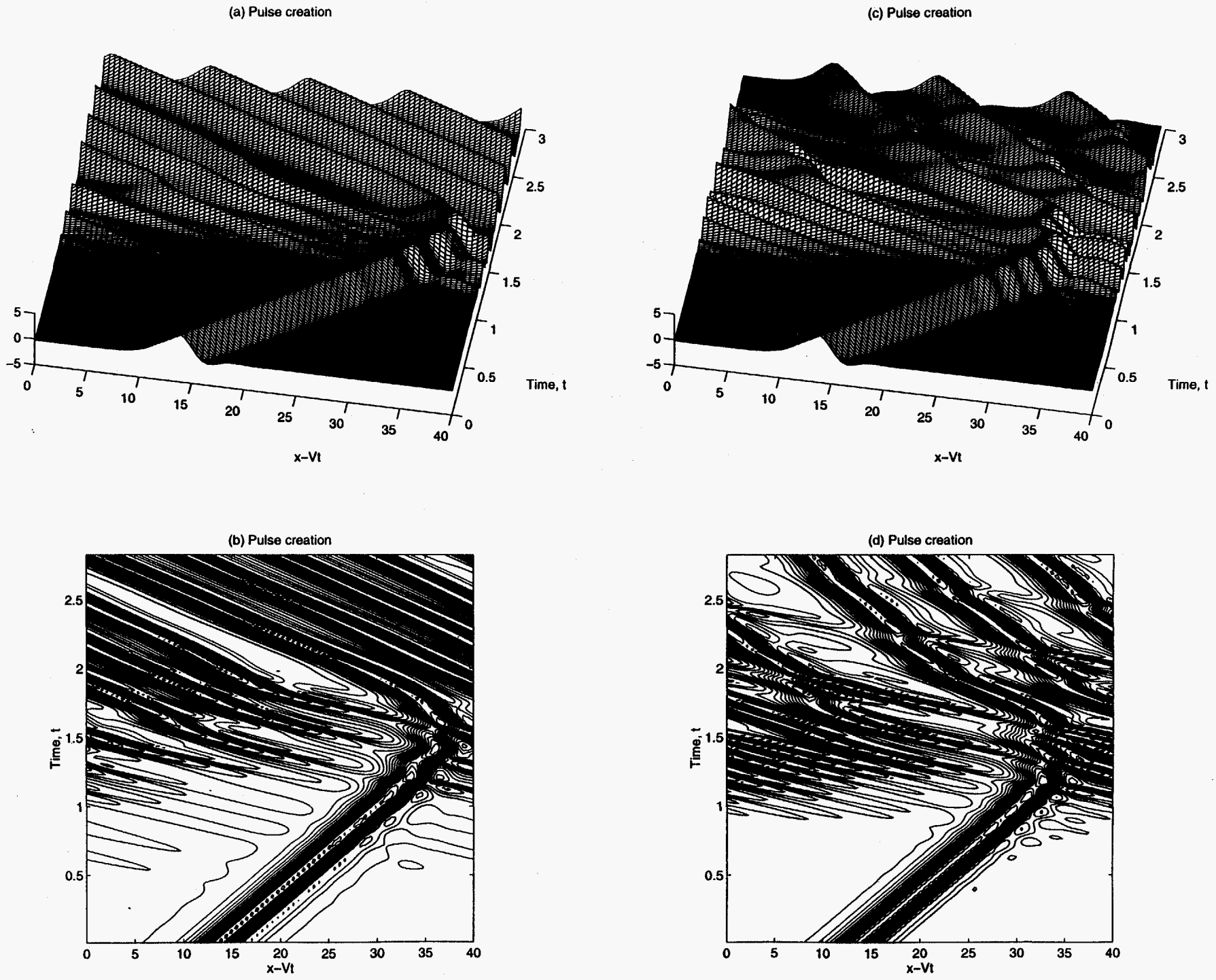
(a) Pulse creation
(c) Pulse creation
(b) Pulse creation
(d) Pulse creation
x–Vt
Time, t

Figure 12

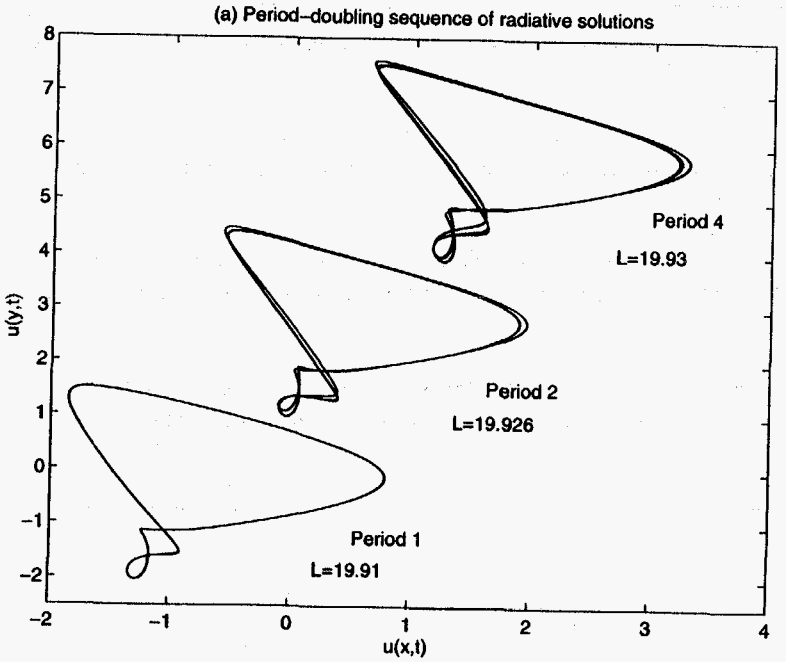
(a) Period–doubling sequence of radiative solutions
Period 4
L=19.93
Period 2
L=19.926
Period 1
L=19.91
u(y,t)
u(x,t)

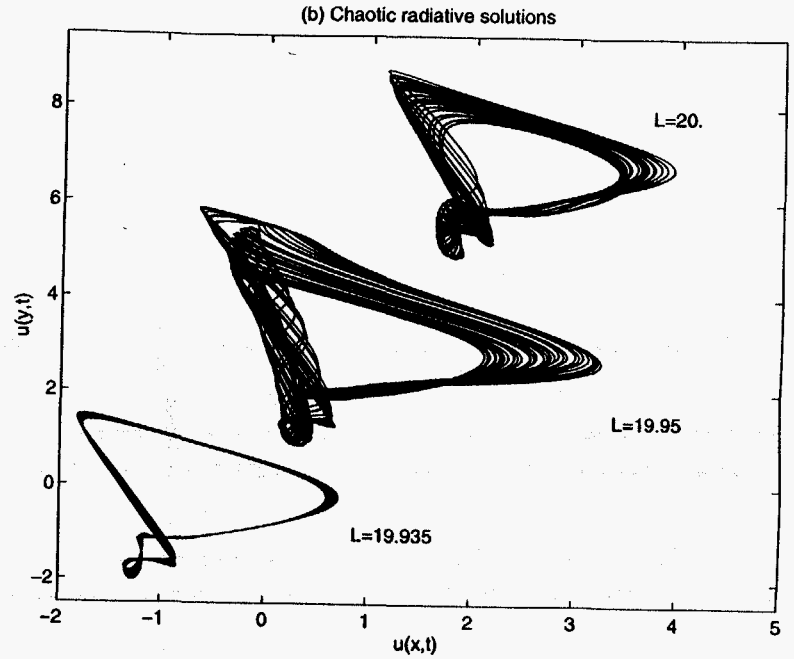
(b) Chaotic radiative solutions
L=20.
L=19.95
L=19.935
u(y,t)
u(x,t)

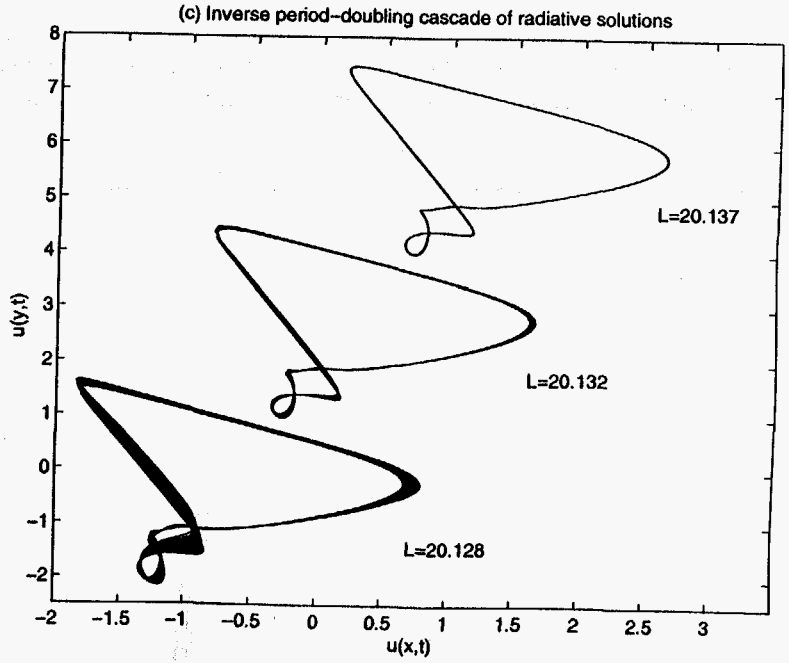
(c) Inverse period–doubling cascade of radiative solutions
L=20.137
L=20.132
L=20.128
u(y,t)
u(x,t)

Figure 13

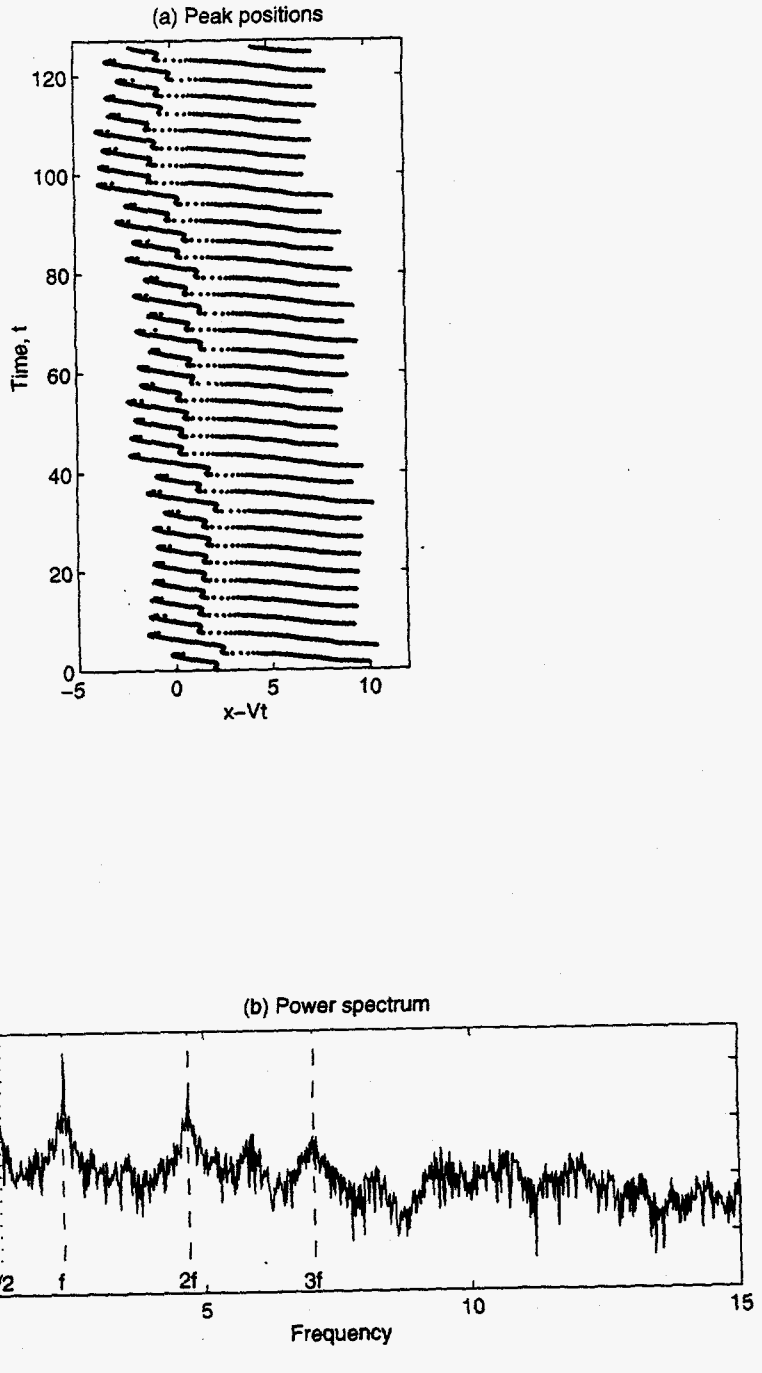
(a) Peak positions
Time, t
x–Vt
120
100
80
60
40
20
0
–5
0
5
10
(b) Power spectrum
Power
Frequency
15
10
5
0
–5
0
5
10
15
1/2
f
2f
3f

Figure 14: Period–doubling cascade of saturated inertial–mode solutions

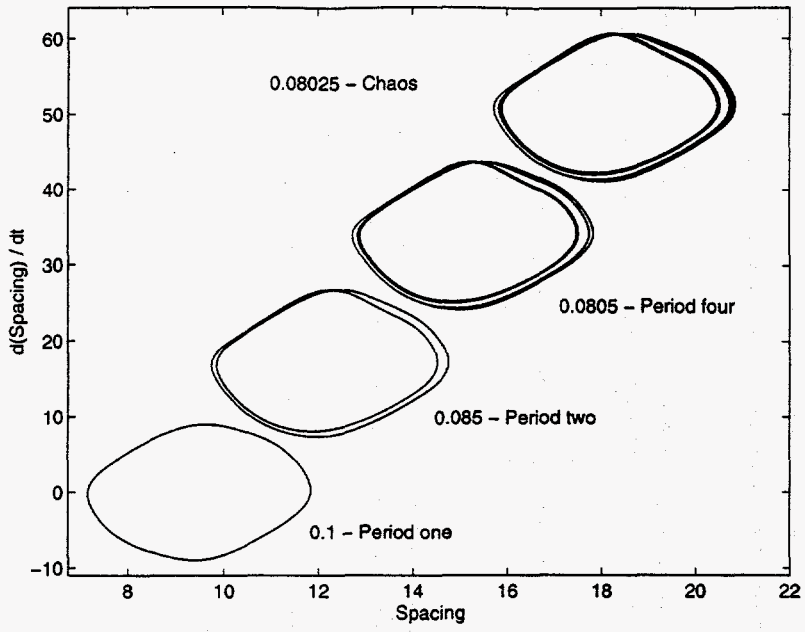

Figure 15

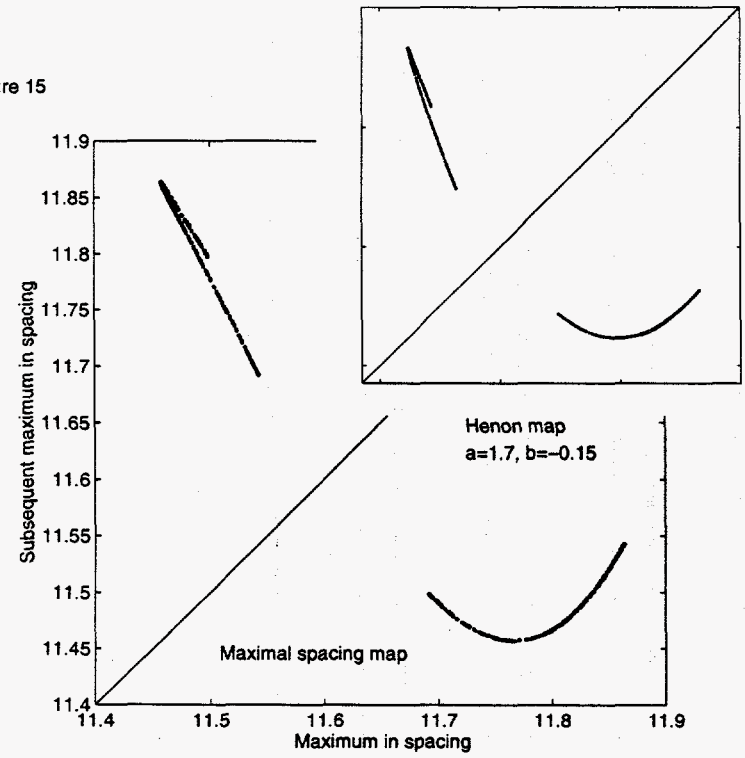

Figure 16

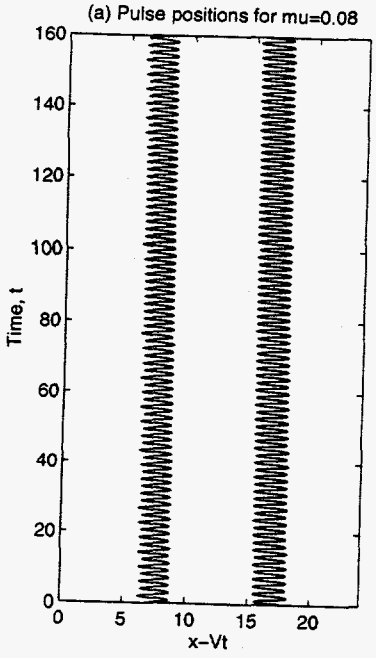
(a) Pulse positions for mu=0.08
Time, t
x-Vt
0
20
40
60
80
100
120
140
160
0
5
10
15
20

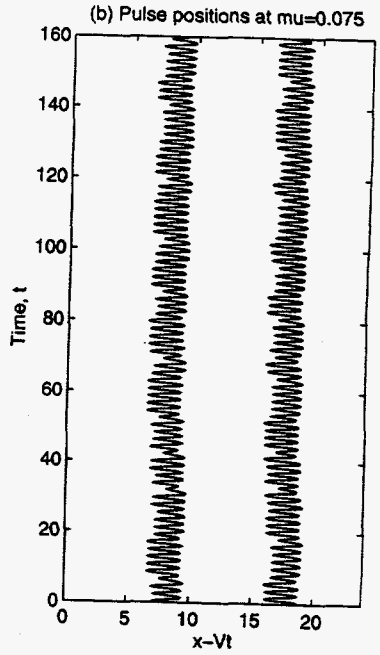
(b) Pulse positions at mu=0.075
Time, t
x-Vt
0
20
40
60
80
100
120
140
160
0
5
10
15
20

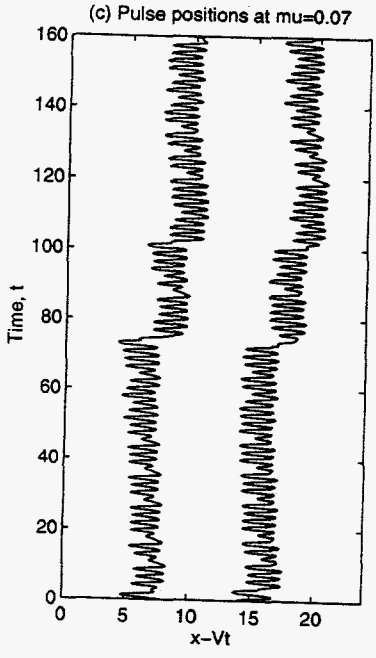
(c) Pulse positions at mu=0.07
Time, t
x-Vt
0
20
40
60
80
100
120
140
160
0
5
10
15
20

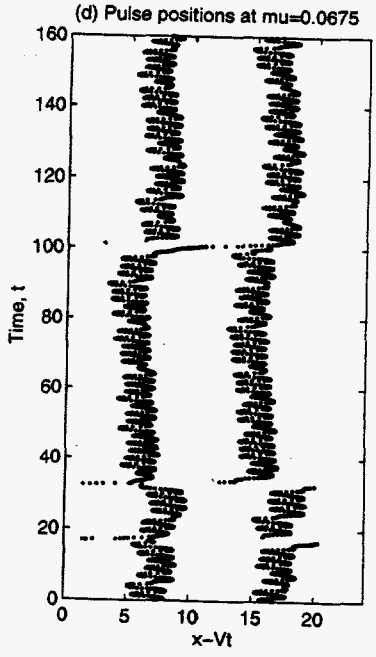
(d) Pulse positions at mu=0.0675
Time, t
x-Vt
0
20
40
60
80
100
120
140
160
0
5
10
15
20

Figure 17

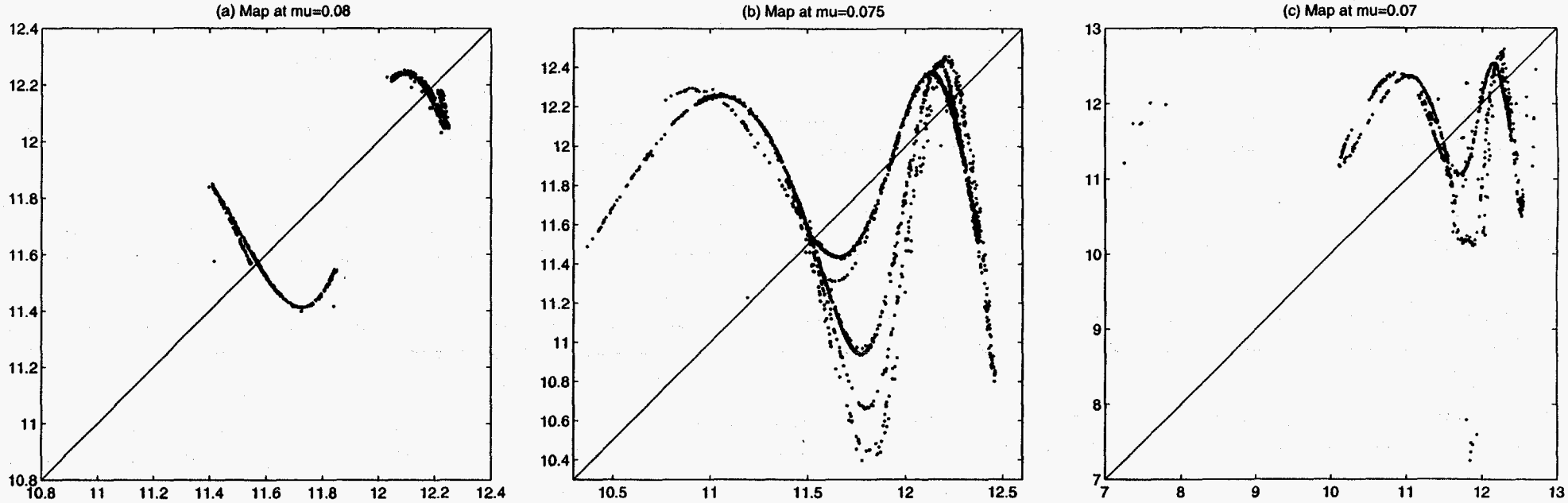
(a) Map at mu=0.08
12.4
12.2
12
11.8
11.6
11.4
11.2
11
10.8
10.8 11 11.2 11.4 11.6 11.8 12 12.2 12.4
(b) Map at mu=0.075
12.4
12.2
12
11.8
11.6
11.4
11.2
11
10.8
10.6
10.4
10.5 11 11.5 12 12.5
(c) Map at mu=0.07
13
12
11
10
9
8
7
7 8 9 10 11 12 13

Figure 18

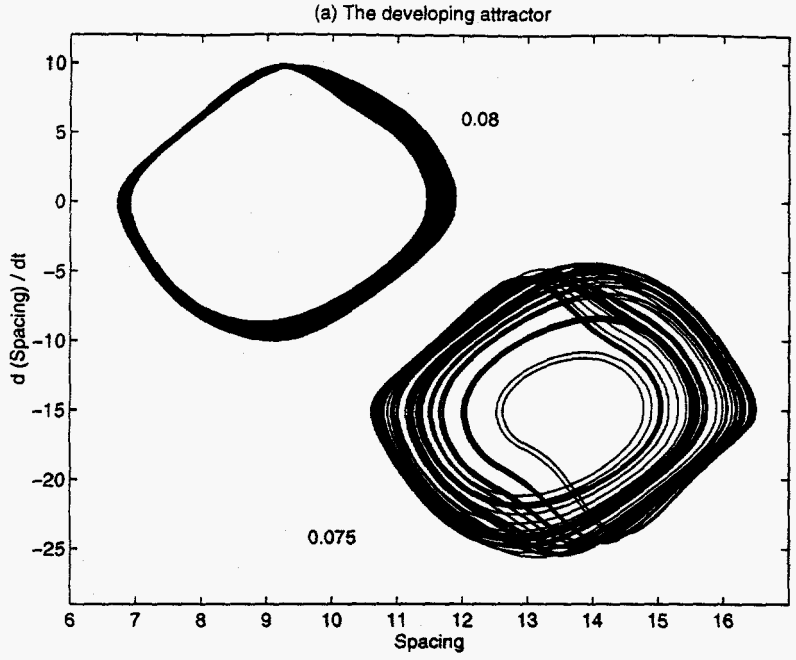
(a) The developing attractor
0.08
0.075
d (Spacing) / dt
Spacing
10
5
0
-5
-10
-15
-20
-25
6
7
8
9
10
11
12
13
14
15
16

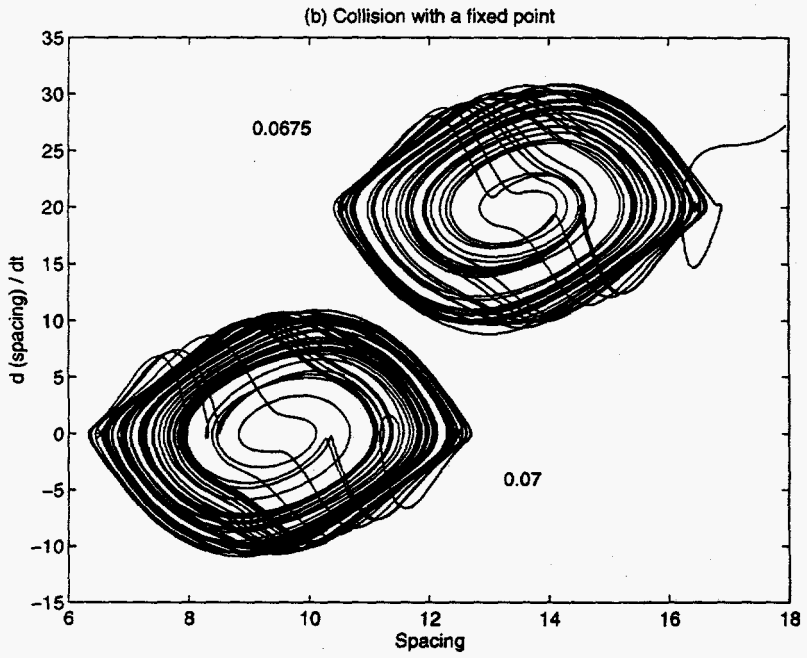
(b) Collision with a fixed point
0.0675
0.07
d (spacing) / dt
Spacing
35
30
25
20
15
10
5
0
-5
-10
-15
6
8
10
12
14
16
18

Figure 19

(a) The annihilation–nucleation event

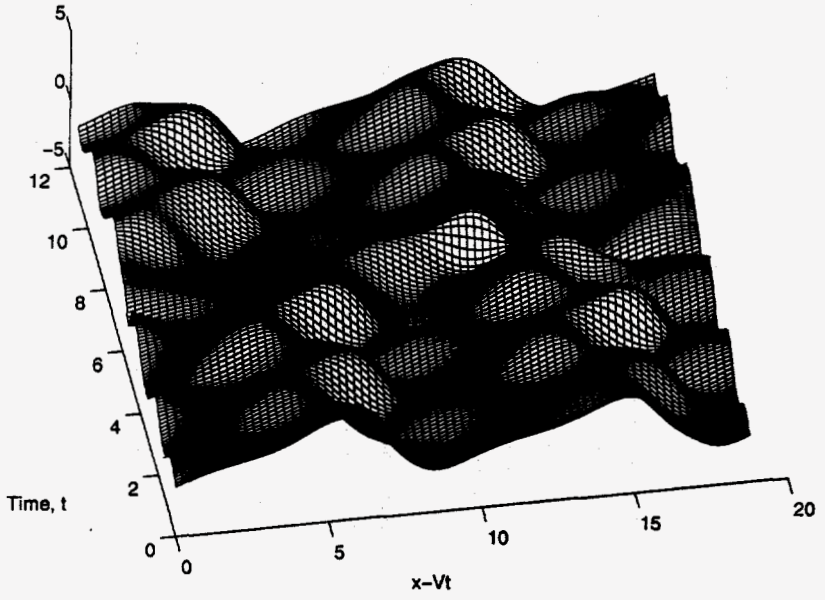

(b) The annihilation–nucleation event

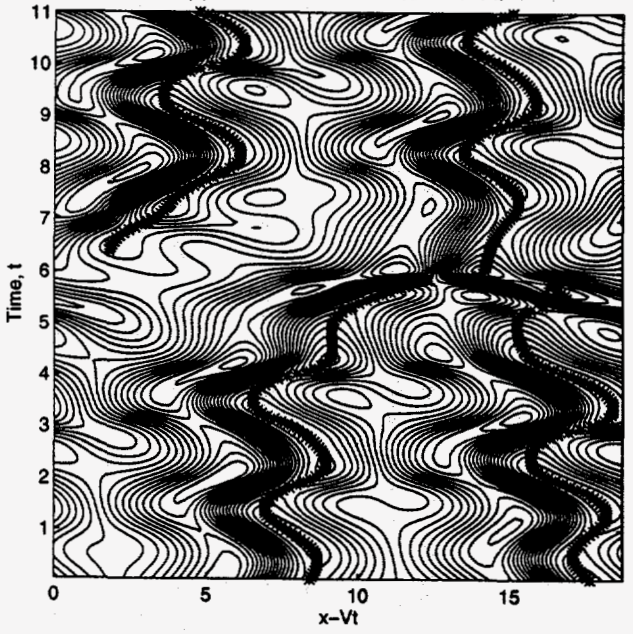

Figure 20

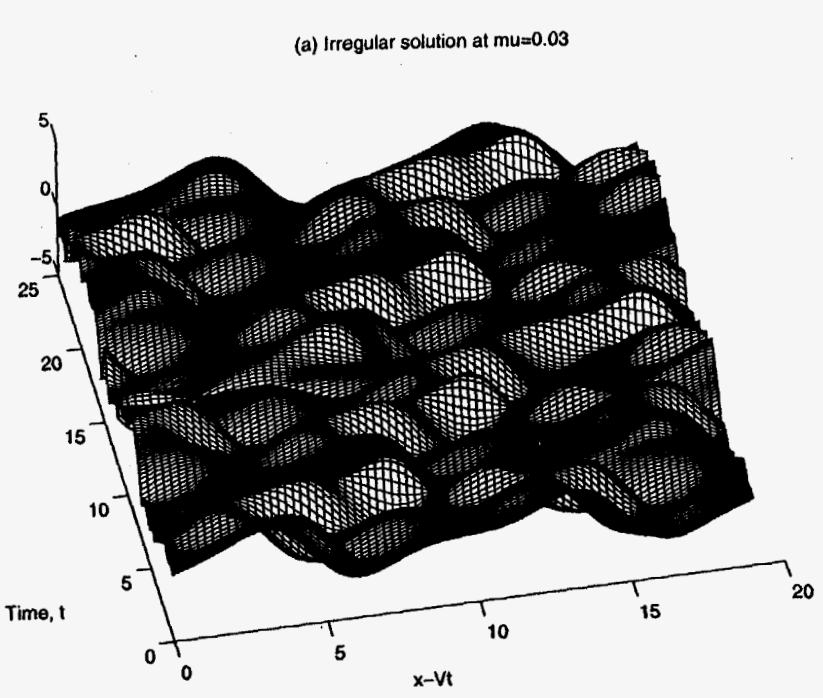
(a) Irregular solution at mu=0.03
Time, t
x–Vt

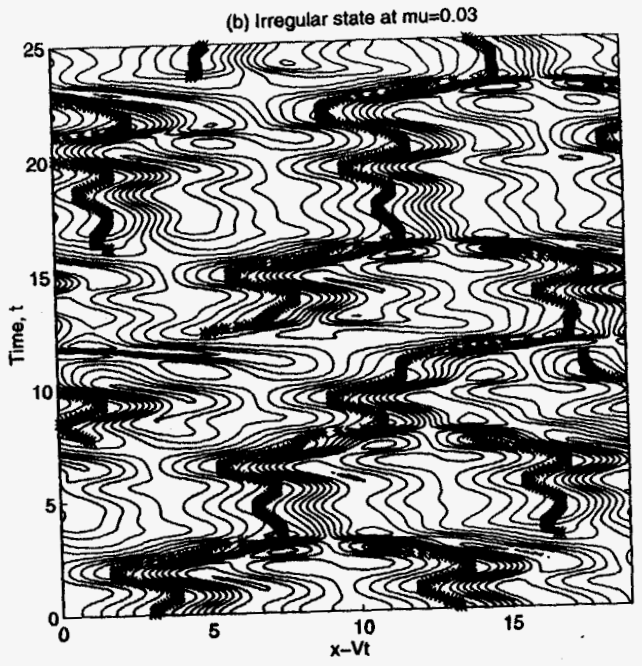
(b) Irregular state at mu=0.03
Time, t
x–Vt

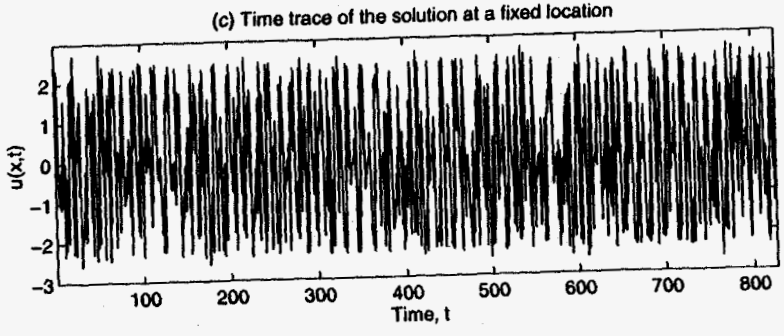
(c) Time trace of the solution at a fixed location
u(x,t)
Time, t

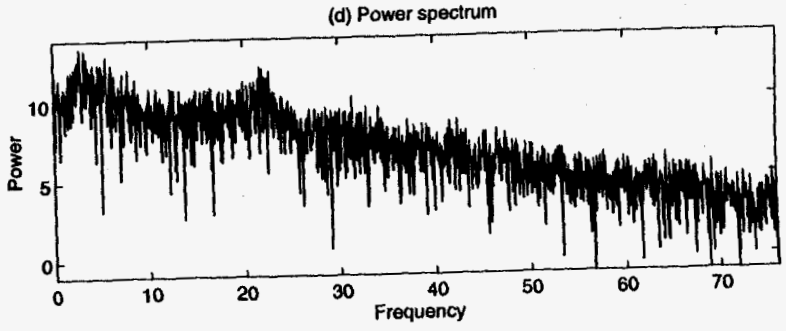
(d) Power spectrum
Power
Frequency

Figure 21

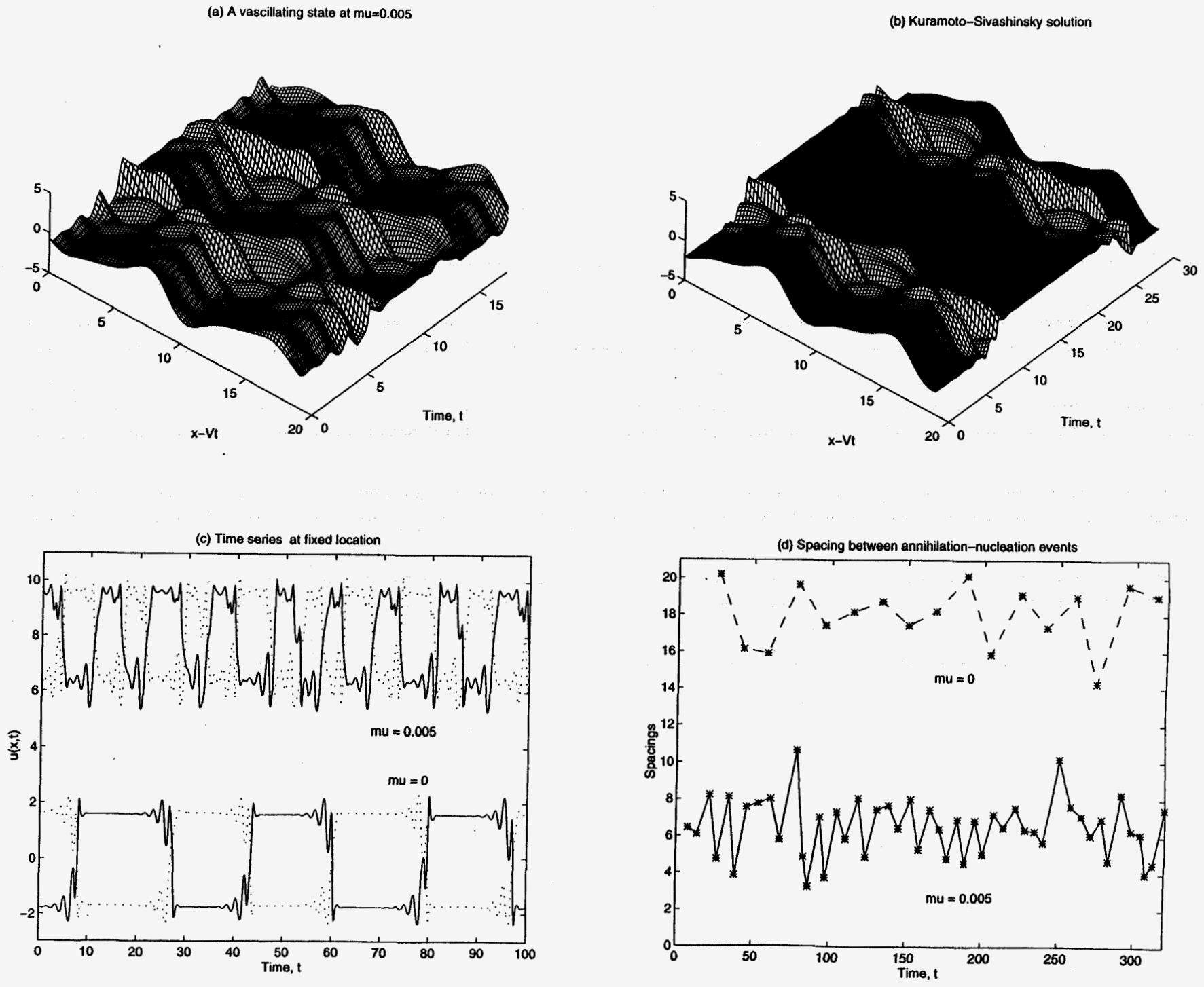
(a) A vascillating state at mu=0.005
x–Vt
Time, t
(b) Kuramoto–Sivashinsky solution
x–Vt
Time, t
(c) Time series at fixed location
u(x,t)
mu = 0.005
mu = 0
Time, t
(d) Spacing between annihilation–nucleation events
Spacings
mu = 0
mu = 0.005
Time, t

Figure 22: Various phase portraits of the Kuramoto–Sivashinsky solution

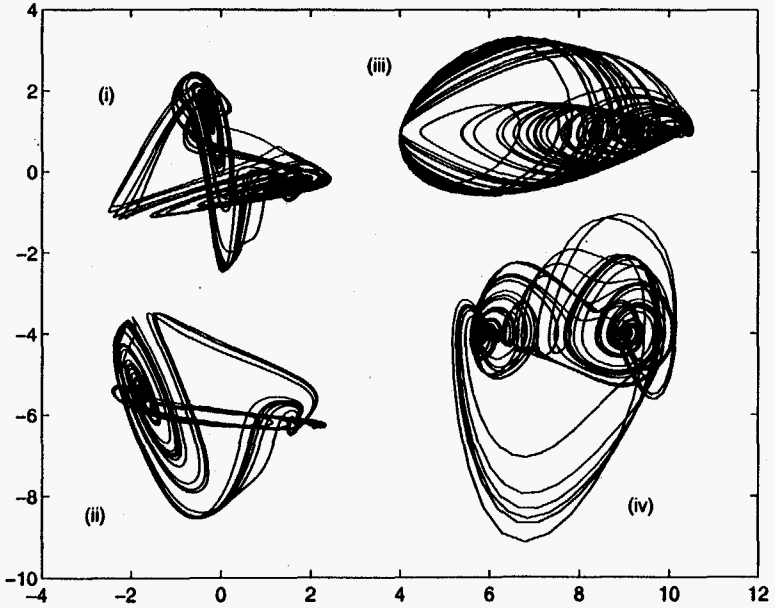

Figure 23: Evolution over longer intervals

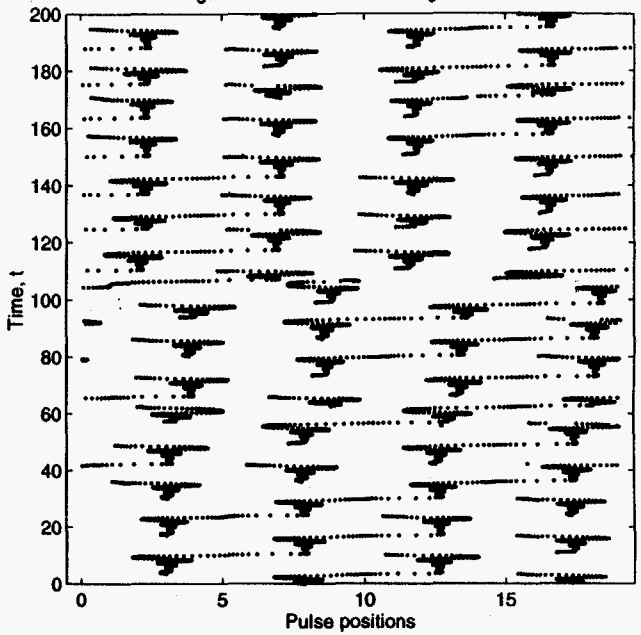

Figure 24: Intermittent patterns at mu=0.1305

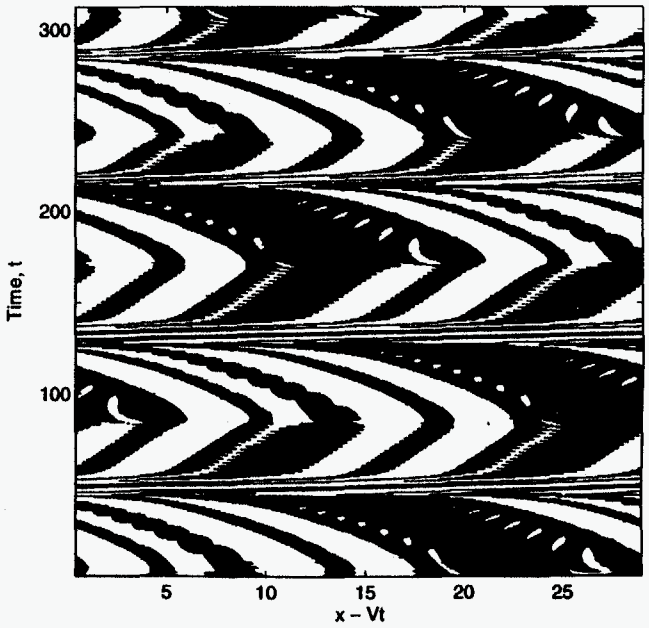

Figure 25(a) Evolution for mu=0, L=29

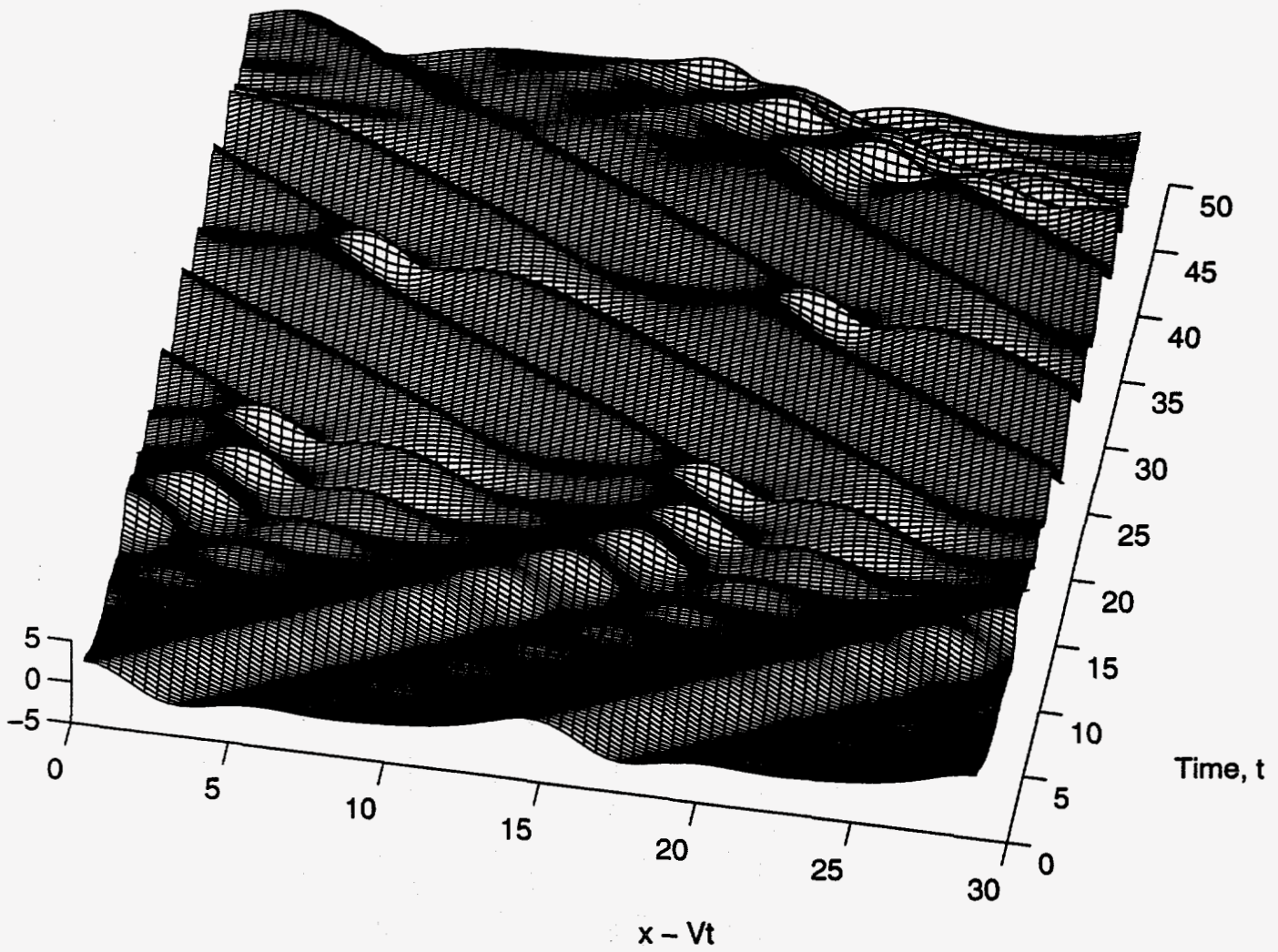

Figure 25(b) Continued evolution for mu=0, L=29

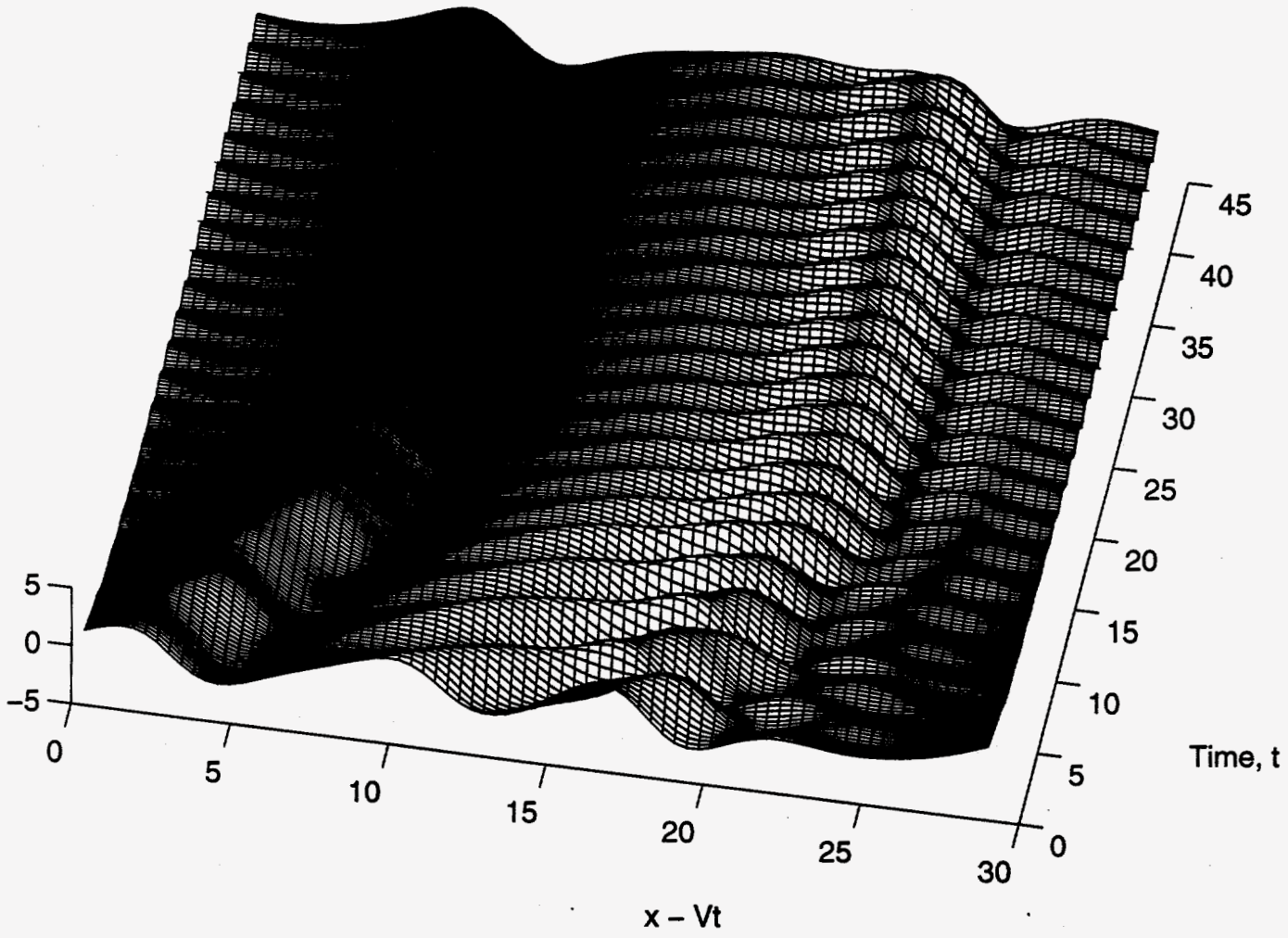

Figure 26: A hard collision